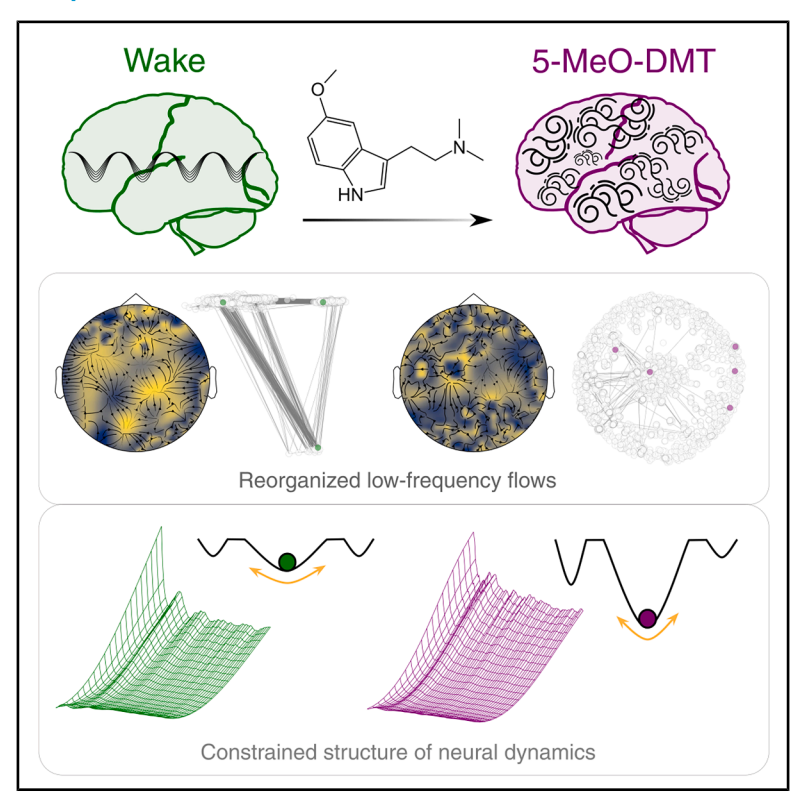
# Complex slow waves in the human brain under 5-MeO-DMT

# Graphical abstract



## **Authors**

George Blackburne, Rosalind G. McAlpine, Marco Fabus, Alberto Liardi, Sunjeev K. Kamboj, Pedro A.M. Mediano, Jeremy I. Skipper

# Correspondence

george.blackburne.18@ucl.ac.uk

## In brief

Blackburne et al. show how the psychedelic drug 5-MeO-DMT affects the human brain. The authors report changes in the spatiotemporal organization of slow waves and find that 5-MeO-DMT pushes human brain dynamics toward a low-dimensional steady state on a steepened energy landscape.

# **Highlights**

- 5-MeO-DMT radically reconfigures human brain activity
- Low-frequency traveling waves become disorganized
- Low-frequency traveling waves reduce forward and backward travel across the cortex
- Broadband dynamics become more stable and lowdimensional on a steepened energy landscape







# **Article**

# Complex slow waves in the human brain under 5-MeO-DMT

George Blackburne, 1,2,6,\* Rosalind G. McAlpine, Marco Fabus, 4,5 Alberto Liardi, Sunjeev K. Kamboj, Pedro A.M. Mediano, 1,2 and Jeremy I. Skipper 1

#### **SUMMARY**

5-methoxy-N,N-dimethyltryptamine (5-MeO-DMT) is a psychedelic drug known for its uniquely profound effects on consciousness; however, it remains unknown how it affects the brain. We collected electroencephalography (EEG) data of 29 healthy individuals before and after inhaling a high dose (12-mg) of vaporized synthetic 5-MeO-DMT. We replicate results from rodents showing amplified low-frequency oscillations but extend these findings by characterizing the complex organization of spatiotemporal fields of neural activity. We find that 5-MeO-DMT radically reorganizes low-frequency flows, causing them to become heterogeneous, viscous, and nonrecurring and to cease their travel forward and backward across the cortex. Further, we find a consequence of this reorganization in broadband activity, which exhibits more stable low-dimensional behavior with increased energy barriers for rapid global shifts. These findings provide a detailed empirical account of how 5-MeO-DMT sculpts human brain dynamics, revealing a set of atypical cortical slowwave behaviors with significant implications for neuroscientific models of serotonergic psychedelics.

## INTRODUCTION

Psychedelic drugs are reentering scientific research as unique and reliable tools for interrogating the neural processes that entail alterations in the structure of subjective experience. <sup>1,2</sup> In tandem, they are being explored as potential treatments for an array of mental health conditions. <sup>3,4</sup> However, 5-methoxy-N,N-dimethyltryptamine (5-MeO-DMT), likely the most profound agent in this class, <sup>5</sup> has remained unstudied in human neuroscience. This is despite its current involvement in clinical trials for the treatment of depression, <sup>6,7</sup> bipolar, <sup>8</sup> and alcohol use disorders. <sup>9</sup>

5-MeO-DMT is a naturally occurring, potent, rapid-acting tryptamine, with its use likely dating back over 1,000 years to South American Tiwanaku ritual practices via insufflation of the trace concentrations contained in *Anadenanthera* seeds. <sup>10,11</sup> Contemporary usage, however, is markedly different, predominantly occurring through either the synthetic form or via the venom secreted from the parotid glands of the *Incilius alvarius* toad. <sup>12</sup> Indeed, it is the high-dose combustion or vaporization and inhalation of these formats through which 5-MeO-DMT has attained its unofficial status as the world's most powerful psychedelic, or the "God molecule."

The experience elicited by inhaled 5-MeO-DMT, like its chemical relative DMT, is characterized by a radical progression, or

"breakthrough," into what is felt as "another dimension," such that sensation becomes detached from consensus reality. 13 However, unlike DMT, this environmental disconnection generally does not typically involve immersion into an overwhelmingly visually intricate geometric space filled with seemingly sentient entities but rather a world entirely lacking the usual axes of variation to structure it. At the peak of the 5-MeO-DMT experience, rudimentary structures of subjective experience, such as time, space, and the self, are felt to be abolished, and a dramatic loss of differentiation ensues. 14 Fully awake, individuals feel they have entered into an ineffable realm of "everything and nothing," where even the inference that they are the subject of the experience is protracted. 15 5-MeO-DMT is therefore a perturbation that renders which of a creature's consciousnessrelated capacities can be online but does not, in the classical sense, "reduce" the level, degree, or intensity of consciousness. 16,17 In other words, 5-MeO-DMT deconstructs, but does not destroy, subjective experience. We propose, therefore, that it be most productively referred to as a "global mode of deconstructed consciousness."

Preclinical work in awake rodents indicates that 5-MeO-DMT elicits its most pronounced effects in augmenting low-frequency rhythms (<4 Hz). 18-21 5-MeO-DMT has been shown to increase the power of low-frequency oscillations in local field potentials (LFPs), with multi-unit recordings showing neural activity to



<sup>&</sup>lt;sup>1</sup>Department of Experimental Psychology, University College London, London, UK

<sup>&</sup>lt;sup>2</sup>Department of Computing, Imperial College London, London, UK

<sup>&</sup>lt;sup>3</sup>Clinical Psychopharmacology Unit, University College London, London, UK

<sup>&</sup>lt;sup>4</sup>School of Medicine and Biomedical Sciences, University of Oxford, Oxford, UK

<sup>&</sup>lt;sup>5</sup>Wellcome Centre for Integrative Neuroimaging, University of Oxford, Oxford, UK

<sup>&</sup>lt;sup>6</sup>Lead contact

<sup>\*</sup>Correspondence: george.blackburne.18@ucl.ac.uk https://doi.org/10.1016/j.celrep.2025.116040



alternate between periods of high firing and generalized silence concurrently to the 1 Hz LFP cycles, while mice freely behave. This hybrid state was therefore dubbed "paradoxical wakefulness," as mice exhibited the canonical neurophysiological signatures of slow-wave sleep (SWS) while awake. The amplification of low-frequency oscillations is thought to be a domaingeneral indicator of loss of consciousness beyond SWS, such as the period of slow-wave activity saturation (SWAS) in general anesthesia and coma patients who are diagnosed with unresponsive wakefulness syndrome. Thus, these results with 5-MeO-DMT challenge the idea that amplified low-frequency rhythms have a one-to-one correspondence with reductions in conscious level.

Simple oscillatory phenomena in the brain are increasingly being empirically understood as univariate symptoms of more complex spatiotemporal propagating patterns, with SWS and SWAS exemplifying this shift in understanding.<sup>26-29</sup> Indeed, there have been recent theoretical and empirical calls to define brain states more generally via wave-like processes, 30-32 though the idea that the brain is a non-stationary system composed of trajectories inextricably structured in space and time is not itself a recent development.33-35 Complex flows, or metastable waves, are transient activity patterns that sweep across the cortex and converge around points of stationarity, termed singularities. These can take on a host of forms, such as sources or sinks, which expand or contract around a point; spirals, which rotate around a point; and saddles, which are usually the superposition of different interacting waves. These patterns have been consistently observed in mesoscopic and macroscopic neural recordings<sup>31,36-40</sup> and are thought to play crucial roles in cortical computation, 41,42 modulating excitation-inhibition balance, 43 memory, 44,45 and perception. 46-48

Thus, a productive approach for the empirical characterization of the effects of 5-MeO-DMT on macroscopic brain dynamics might lie in understanding how complex low-frequency flows are reorganized. We hypothesized that while 5-MeO-DMT may look analogous to states of unconsciousness from a univariate oscillatory perspective, given its salient phenomenology, it should look strikingly different from a more comprehensive spatiotemporal standpoint. Instead of inducing more coherent, durable, and stereotyped global low-frequency flow structures, like in anesthesia, 26,28,49 we predicted that 5-MeO-DMT would induce the opposite effect, that is, a state of resolute complex low-frequency incoherence, with disjointed and viscous flows limiting the emergence of global propagating patterns able to spread across the cortex. We hypothesized that there would be a greater occurrence of localized low-frequency patterns with differing directions and speeds that possess short lifetimes and bear little resemblance to each other over time. In sum, we expected that 5-MeO-DMT would upset the backbone of cortical dynamics with "broken," rather than tidal, waves.

Importantly, one should ask what such low-frequency changes functionally imply for statistical motifs of broadband (wide frequency) brain dynamics. Owing to the expected dominance of slow potentials, we predicted that the intrinsic timescales of the cortex would shift toward a slower regime and that excursions from similar activity states would depart from each other more tardily. Crucially, if slow spatiotemporal flows

are disorganized, the brain may be less able to effectively orchestrate large rapid global amplitude reconfigurations, thus increasing the steady-state residence and stability of broadband cortical dynamics. For Given this, broadband responses may be forced from their large population space onto an unusual and simpler sub-space. Put simply, these flows may curb the degrees of freedom of the brain. This bounding of the system's dimensionality could distort and ablate the typical construction of neural representations a such, the individual's model of the world should collapse in parameters, resulting in the deconstruction of subjective experience.

We investigate these predictions by collecting electroencephalography (EEG) data of individuals (N=29) before and immediately after inhaling a high-dose (12-mg) of vaporized synthetic 5-MeO-DMT in a naturalistic setting. We first replicate recent work in rodents on the power of low-frequency oscillations but extend this by performing a suite of analyses characterizing alterations in the organization and dynamics of complex low-frequency spatiotemporal flows of neural activity. We then complement this by assessing the statistical behavior of broadband signals across the cortex in terms of their intrinsic timescales, separation rates, underlying energy landscape, and dimensionality. In doing so, we provide a detailed account of the neuroscience of 5-MeO-DMT in humans.

#### **RESULTS**

#### **Slow oscillations**

Given the lack of 5-MeO-DMT research in humans, we begin by assessing the frequency content of our 64-channel EEG data (Figure S1). The signature effect of 5-MeO-DMT in mice has been the amplification of low-frequency oscillations (<4 Hz), with no clear effect observed on the power of alpha oscillations, the deflation of which is currently considered the neurophysiological signature of psychedelic drug effects in humans. <sup>52-65</sup>

To enable robust time-frequency representation of cortical signals, we use empirical mode decomposition (EMD). We do so because canonical methods, such as the Fourier transform (FT), can provide unreliable estimates when signals are noisy, non-sinusoidal, and non-stationary, as is routinely seen in neural recordings. 66-71 As an illustration, a slightly non-linear high-delta (4 Hz) oscillation can be mistaken to contain a low-alpha (8 Hz) rhythm if the FT is applied due to harmonic effects (Figure S2). Therefore, we use EMD to iteratively sift out the intrinsic basis functions of cortical signals without assuming they are sinusoidal or static. We repeat results with multitaper fast Fourier transform (FFT) in Figure S3 and additionally provide band-passed amplitude distributions in Figure S4. Here, we apply EMD and the Hilbert-Huang transform (HHT) to the epoched data in the range of 0.5-50 Hz (n = 19, 10 were excluded due to movement artifacts) to maximize the number of viable participants. The nonlinear power spectrum is taken as the sum across instantaneous frequencies (IFs) over intrinsic mode functions (IMFs), normalized by their density.

5-MeO-DMT shifts the power spectra of cortical signals at its antipodes. Slow (<1.5 Hz) and fast (>20 Hz) oscillations rapidly rise in power within 20 s after drug inhalation and decay after 8–10 min (Figures 1A and 1D; Figures S5 and S6), coincident

# **Article**



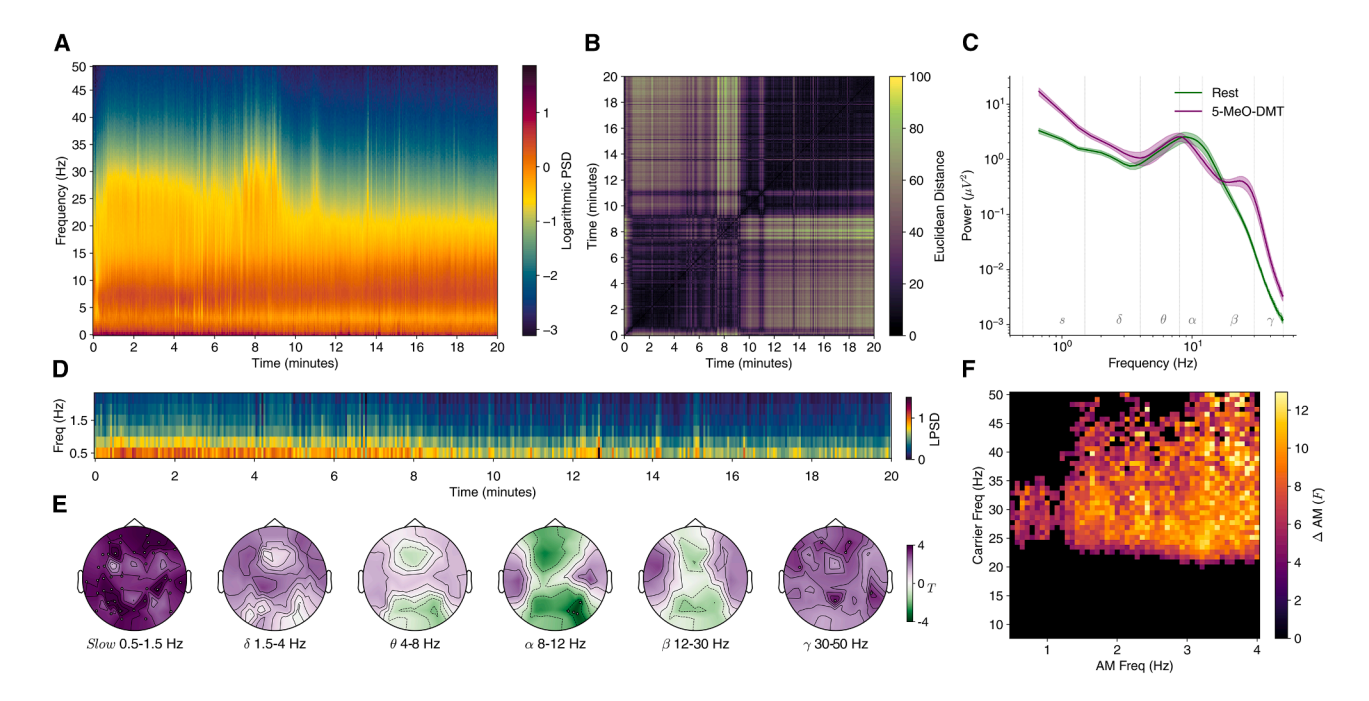


Figure 1. 5-MeO-DMT induces diffuse high-amplitude slow oscillations

(A) Average time-frequency power spectral density (PSD) for the 20 min post-inhalation of 5-MeO-DMT, derived via empirical mode decomposition and the Hilbert-Huang transform.

- (B) Euclidean distance between average power spectra vectors at each epoch with every other epoch. Darker colors indicate more similar spectra between time points.
- (C) Time-averaged power spectra for eyes-closed baseline period and estimated peak 5-MeO-DMT at 1.5-2.5 min (mean ± SEM).
- (D) Focused low-frequency spectrogram.
- (E) Scalp topographic statistical maps for t test comparing the two conditions per frequency band and electrode, with electrodes representing significant differences (p < 0.05, FDR-corrected Benjamini-Hochberg procedure). Purple indicates increases under 5-MeO-DMT, and green indicates reductions.
- (F) Holospectrum statistical map for ANOVA comparing the two conditions, with significant clusters colored (p < 0.05, cluster corrected).

with the expected rise and decay of drug effects. To examine whether alterations in spectra can be seen to track the expected duration of drug effects, we calculate the Euclidian distance between the average power spectra for each epoch and every other epoch. Indeed, we see that the first 4 min are marked by a particularly constant spectral profile (Figure 1B).

Examining the estimated peak of the drug effect (1.5-2.5 min) reveals a stark effect at low frequencies. We find that the mean power of the lowest-frequency bin (0.5 Hz) increases by 415% compared to the baseline (Figure 1C). This effect is also seen when comparing the onset of drug effects (0-1 min) to the baseline and when comparing the peak of the drug effects to the tail after the acute effects have worn off (19-20 min) (Figure S6). These amplified slow oscillations (0.5-1.5 Hz) are spatially distributed, with increases occurring over frontal, parietal, temporal, central, and occipital electrodes (Figure 1E; max: PO3 T=5.104,  $p_{FDR}=0.011$ ,  $BF_{10}=365.623$ , and d=1.472).

Inspecting higher-frequency changes, we observe distributed but weaker increases in gamma oscillations at the estimated peak (Figure 1E; max: Pz T=3.750,  $p_{FDR}=0.001$ ,  $BF_{10}=26.542$ , and d=1.025). As the expected endpoint of the experience is arriving, between 7.5 and 9 min, there is a sudden jump in high-frequency oscillations (Figure 1A). Notably, we see that alpha oscillations are not robustly reduced across every area of the cortex with the large effect sizes seen with other psy-

chedelic compounds<sup>64</sup> (Figure 1E). When parameterizing the peaks of the average power spectra with Gaussians,<sup>72</sup> we find no significant change in alpha oscillatory power (T=0.851,  $p_{FDR}=0.411$ ,  $BF_{10}=0.379$ , and d=0.416) but a significant reduction in the peak frequency (T=-2.898,  $p_{FDR}=0.023$ ,  $BF_{10}=4.576$ , and d=1.097). This lack of effect on alpha oscillatory power is also the case when compared to 19 min after drug ingestion, which is when the acute effects have worn off ( $p_{FDR}=0.372$ ), and when comparing the onset of drug effects to the baseline ( $p_{FDR}=0.874$ ) (Figure S6). Examining the topography of alpha power changes, we find significant reductions over the right parietal-occipital cortex (Pz:  $p_{FDR}=0.030$ ) but also increases in alpha power over the temporal lobes approaching significance (T8:  $p_{FDR}=0.052$ ).

Finally, we investigate whether fast oscillations can themselves be understood in terms of slow oscillations. Specifically, we test if there is greater amplitude modulation of high-frequency content by low-frequency content under 5-MeO-DMT, as evidenced by changes in their holospectrum. Indeed, we find that carrier rhythms in the range of 20–50 Hz exhibit significantly greater fluctuations in power between 0.2 and 4 Hz under 5-MeO-DMT (Figure 1F;  $\rho=0.005$  ANOVA cluster-level permutation).

In sum, these results provide evidence for increases in the power of slow oscillations in the human brain under 5-MeO-DMT,



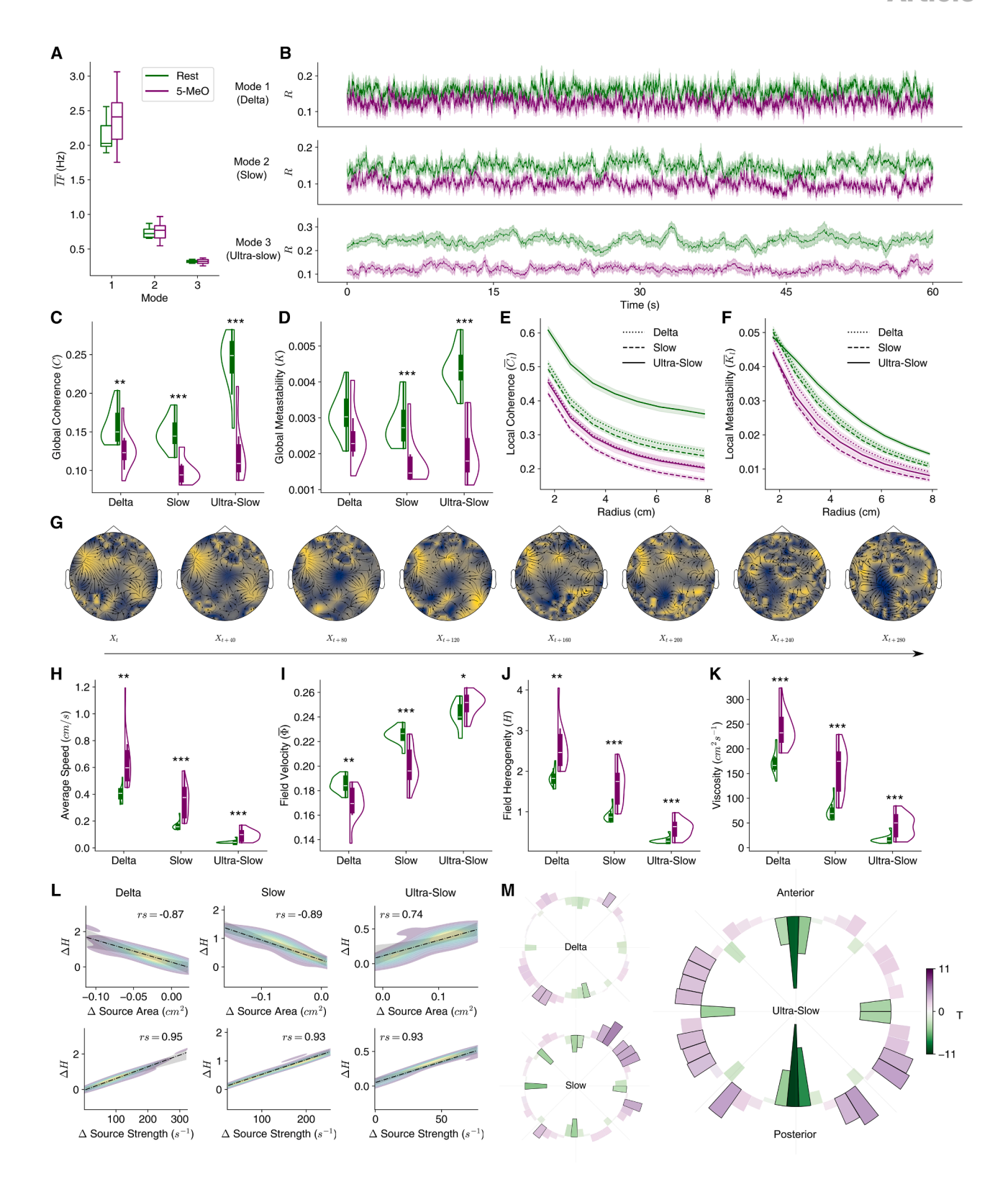


Figure 2. 5-MeO-DMT reorganizes patterns of complex low-frequency flow (A) Mean instantaneous frequency for each intrinsic mode function (IMF).

(B) Instantaneous global phase coherence for each IMF (mean ± SEM).

# **Article**



replicating results from rodents, <sup>18-20</sup> as well as providing evidence that substantial whole-brain loss of alpha power may not be as essential for the 5-MeO-DMT experience, in contrast to other classical psychedelics.

#### **Complex slow waves**

Moving past characterizing the power of univariate rhythmic fluctuations in neural activity in the two conditions, we characterize multivariate macroscopic propagating patterns with particular temporal motifs. We do this by adopting the mathematics of flow velocity from fluid dynamics. We first perform EMD on the continuous signals from the peak window for those participants who have it artifact free (1.5–2.5 min post-ingestion, n = 13) to maximize detection of the low-frequency cycles, obtaining six time-evolving oscillatory IMFs for each electrode. These modes have mean IFs of 16.398  $\pm$  1.104, 6.797  $\pm$  0.290,  $2.270 \pm 0.093$ ,  $0.741 \pm 0.028$ ,  $0.319 \pm 0.007$ , and  $0.133 \pm$ 0.004, respectively (all in Hz). Since our interest is low-frequency modes, we only analyze the third, fourth, and fifth modes, excluding the sixth as a residual artifactual drift, and refer to these as delta, slow, and ultra-slow throughout. The mean IFs of these modes do not significantly change between conditions (Figure 2A; delta: T = 3.012 and  $p_{FDR} = 0.065$ ; slow: T = 0.462and  $p_{FDR} = 1$ ; and ultra-slow: T = -0.112 and  $p_{FDR} = 1$ ). After interpolation of the instantaneous amplitude and phase of the modes onto a uniform  $32 \times 32$  scalp grid mimicking the pixels from optical imaging voltage grids, 49 we obtain the velocity field at each sample for each mode and condition (see STAR Methods). See Figure 2G for an example velocity field evolving over time for mode 2 under 5-MeO-DMT. As expected, we detect continuous and complex propagating spatiotemporal patterns in both conditions but with markedly different structures and dynamics (Figures 2B-2M).

Specifically assessing alterations in phase interactions of the field via a Kuramoto-like formalism (see STAR Methods), we find that 5-MeO-DMT reduces the phase synchrony (global coherence) of low-frequency phase fields (Figure 2C; delta:  $p_{FDR}=0.010$ , slow:  $p_{FDR}=2.07\times10^{-5}$ , and ultra-slow:  $p_{FDR}=8.73\times10^{-7}$ ) and also results in less variance in this synchrony over time (global metastability) (Figure 2D; delta:  $p_{FDR}=0.080$ , slow:  $p_{FDR}=5.96\times10^{-4}$ , and ultra-slow:  $p_{FDR}=8.73\times10^{-7}$ ). We find that this is also the case locally, across radii ranging from 1.75 to 7.875 cm in increments of 0.875 cm for both coherence (Figure 2E) and metastability (Figure 2F) (see Table S2 for full sta-

tistics). We also find that 5-MeO-DMT reduces the topographic variance of local coherence and metastability, leading to a collapsed hierarchy of synchronization properties (Figure S7). Taken together, these results show that 5-MeO-DMT induces a state of persistent low-frequency desynchronization.

Examining the velocity fields further, we find that 5-MeO-DMT causes waves to travel faster on average (Figure 2H; delta:  $p_{FDR} = 0.002$ , slow:  $p_{FDR} = 1.49 \times 10^{-4}$ , and ultra-slow:  $p_{FDR} = 2.61 \times 10^{-4}$ ). However, this largely reflects disorganized and spatially circumscribed flow since, globally, the field exhibits less directional alignment and collective motion, as shown by reductions in the field normalized velocity for delta and slow waves (Figure 2I; delta:  $p_{FDR} = 0.003$  and slow:  $p_{FDR} = 7.19 \times 10^{-5}$ ). However, the opposite is true for ultra-slow waves (Figure 2I;  $p_{FDR} = 0.026$ ). Supporting the idea that flow becomes more fragmented, we find that velocity fields become significantly more spatially heterogeneous (Figure 2J; delta:  $p_{FDR} = 0.001$ , slow:  $p_{FDR} = 1.49 \times 10^{-4}$ , and ultra-slow:  $p_{FDR} = 1.49 \times 10^{-4}$ ) (see Table S3 for full statistics). We predicted that this would be the result of decreases in the area occupied by flow sources and increases in the strength (divergence) exerted by flow sources. Indeed, we show that such decreases in the area of sources and increases in the strength of sources strongly correlate with the observed changes in field heterogeneity, with the lowest rs = 0.74 (Figure 2L) (see Table S6 for full singularity statistics).

We further confirm the "provincializing" effects of 5-MeO-DMT on low-frequency flow by showing that it becomes more viscous, revealing that the diffusion of neural activity across the cortex at this timescale is significantly hampered by the drug (Figure 2K; delta:  $p_{FDR} = 5.23 \times 10^{-4}$ , slow:  $p_{FDR} = 2.34 \times 10^{-4}$ , and ultra-slow:  $p_{FDR} = 7.35 \times 10^{-4}$ ). In sum, 5-MeO-DMT induces a state of disorganized low-frequency flow, giving rise to greater local patterns with diverse shapes, directions, and speeds. These flows collectively diminish the emergence of global propagating patterns with specific paths across the cortex.

To directly assess changes in the path of waves across the cortex, we obtain the angle of each grid element on the scalp via the inverse of the tangent of their x and y directional vectors. We bin the  $2\pi$  complete angle of directions into 50 bins and contrast each bin between conditions, finding that 5-MeO-DMT significantly alters wave travel directionality (Figure 2M). We find that slow and ultra-slow waves travel significantly less in true anterior, posterior, and lateral directions. Interestingly,

- (C) Global phase coherence for each IMF.
- (D) Global phase metastability for each IMF.
- (E) Local phase coherence for each IMF across radii (mean ± SEM).
- (F) Local phase metastability for each IMF across radii (mean ± SEM).
- (G) Example velocity field for mode 2 from a representative participant over the course of 560 ms during estimated peak of 5-MeO-DMT.
- (H) Mean wave speed for each IMF.
- (I) Average normalized velocity of the velocity field for each IMF.
- (J) Average heterogeneity of the velocity field for each IMF.
- (K) Viscosity of the velocity field for each IMF.
- (L) Correlations between changes in field heterogeneity with changes in source area (top row) and source strength (bottom row) for each IMF (columns). Change scores are 5-MeO-DMT minus the resting rate.
- (M) Changes in the direction of flow for each IMF across the cortex. Bin position indicates direction, and bin orientation indicates change. Inward pointing bins indicate reduced travel under 5-MeO-DMT. t test p < 0.05 FDR-corrected bins are indicated with black borders.
- $^*p$  < 0.05,  $^{**}p$  < 0.01, and  $^{***}p$  < 0.001, FDR-corrected Benjamini-Hochberg procedure.



we observe that all modes instead increase their travel in an intercardinal fashion (Figure 2M). The loss of canonical forward-and backward-traveling waves is particularly striking in the case of ultra-slow waves (Figure 2M; anterior travel: T=-10.375,  $p_{FDR}=3.61\times10^{-5}$ ,  $BF_{10}=6.11\times10^{4}$ , and d=2.639; posterior travel: T=-9.065,  $p_{FDR}=7.67\times10^{-5}$ ,  $BF_{10}=1.66\times10^{4}$ , and d=2.648) (see Table S4 for full statistics). Thus, 5-MeO-DMT reorganizes wave travel and specifically diminishes forward- and backward-traveling slow waves.

Visual inspection of velocity fields at the baseline indicated that field patterns were persistent and frequently reoccurred. However, under 5-MeO-DMT, patterns appeared to have shorter dwell times, with future patterns noticeably more dissimilar to past ones. To specifically test such alterations in the temporal dynamics of low-frequency flows, we compute recurrence matrices for the velocity fields (see STAR Methods). Figures 3A and 3B show example network plots for the first 1/4 (15 s) of the recurrence network for mode 2 from a representative participant. Figure 3C shows the same for the remaining participants. Networks are plotted according to their community structure, with proximity reflecting edge density. In other words, peripheral points reflect unique patterns that are rarely, if ever, revisited. The 5-MeO-DMT recurrence networks can be seen to be scattered and less interconnected, as evidenced by the average degree distributions for each condition in Figure 3D. The mean degree of the recurrence network is significantly reduced by 5-MeO-DMT for all three modes (delta:  $p_{FDR} = 1.38 \times 10^{-4}$ , slow:  $p_{FDR} = 4.21 \times 10^{-6}$ , and ultra-slow:  $p_{FDR} = 4.21 \times 10^{-6}$ ). Indeed, we also see that the number of communities in the recurrence network significantly increases under 5-MeO-DMT (Figure 3E; delta:  $p_{FDR} = 6.89 \times$  $10^{-5}$ , slow:  $p_{FDR} = 0.003$ , and ultra-slow:  $p_{FDR} = 0.033$ ), indicating an increase in the number of unique field patterns. Finally we see that the global efficiency of the network, representing how effectively flow patterns are exchanged between the past and the future, is significantly reduced by 5-MeO-DMT for all three modes (delta:  $p_{FDR} = 0.001$ , slow:  $p_{FDR} = 6.61 \times 10^{-5}$ , and ultraslow:  $p_{FDR} = 2.32 \times 10^{-5}$ ) (see Table S5 for full statistics). In sum, 5-MeO-DMT makes low-frequency flow fields less recurrent and less structured over time.

To test for changes in specific patterns, we classify singularities as either unstable node (sources), stable node (sinks), unstable focus (spiral out), stable focus (spiral in), or saddle waves (see STAR Methods; Figure 3G) and calculate their dynamical properties. We find that 5-MeO-DMT significantly reduces the average lifetime of every pattern of delta and slow waves while engendering a mixed effect on ultra-slow waves, reducing the endurance of nodes but increasing the endurance of spirals and saddles (Figure 3H; delta max, S-Focus: T=-5.880,  $p_{FDR}=3.31\times10^{-4}$ , and BF=371.185; slow max, S-Node: T=-8.757,  $p_{FDR}=6.63\times10^{-5}$ , and  $BF=1.20\times10^{4}$ ; and ultra-slow max: saddle, T=5.463,  $p_{FDR}=5.42\times10^{-4}$ , and BF=209.142) (see Table S7 and Figure S9 for extended statistics). Overall, these results show that 5-MeO-DMT disrupts canonical patterns of low-frequency flow.

#### **Broadband stability**

We predicted that a potential consequence of these low-frequency alterations and a potential cause of the structurally constrained experience induced by the drug would be that broadband neural activity would be forced onto an unusual manifold, where large global shifts are prohibited. We expected that broadband signals would, on average, exhibit slower, more stable low-dimensional behavior, with increased energetic costs for major deviations.

First, we assessed the average decay time of the automutual information (AMI) function, a measure of the intrinsic timescale of neural activity, and found that this doubles under 5-MeO-DMT from 221.9  $\pm$  72.6 to 495.3  $\pm$  94.7 ms (Figure 4A;  $p_{EDB}$  = 0.018), an effect robust to parameter choices (Figure S10). Thus, 5-MeO-DMT makes broadband activity exhibit more regular trends and long-term dependence. We then compute the maximum Lyapunov exponent, a measure of the average separation rate of neighboring points in phase space, and find a weak but significant reduction ( $\lambda_{max}$ ) (Figure 4B;  $\rho_{FDR} = 0.046$ ) (see Table S8 for full statistics). Thus, 5-MeO-DMT makes cortical dynamics more stable by decreasing its sensitivity to initial conditions. We next tested whether cortical dynamics would be easier to explain via principal-component analysis with singular value decomposition. We indeed show that the variance explained (the eigenvalue) is significantly greater for 5-MeO-DMT for each component (eigenvector) (Figure 4C;  $PC_1$   $p_{FDR}$  = 0.027) (see Table S9 for full statistics), indicating that the brain under 5-MeO-DMT indeed exhibits more low-dimensional behavior.

Finally, we examine whether this slow, stable low-dimensional broadband behavior can be cashed out in the language of statistical mechanics as alterations in the topography of a putative energy landscape of cortical dynamics. Here, energy represents the ability of the brain to move from one activity state to another at a particular timescale and is operationalized as the inverse probability of a mean-squared displacement (MSD) in global neural activity of a particular size as a function of time<sup>50</sup> (Figures 4E and 4F). Given the hypothesis that 5-MeO-DMT pushes the brain into an unusual functional sub-space, we expected that 5-MeO-DMT would "protect" the brain from major deviations in neural activity. Indeed, we find that 5-MeO-DMT significantly increases the energy requirement of large-scale deviations (>3 MSD) (max T = 5.527,  $p_{FDR} = 0.001$ ,  $BF_{10} =$ 228.686, and d = 1.193) while also making minor shifts (<1.5 MSD) easier to attain (max T = -4.628,  $p_{FDR} = 0.002$ ,  $BF_{10} =$ 62.859, and d = 1.307) (see Table S10 for full statistics; Figure 4D). We also use non-linear least squares to fit  $e^{m \cdot x}$  curves to our 2D landscape functions and find that 5-MeO-DMT significantly increases the slope of the estimated curve ( $p = 1.58 \times$ 10<sup>-4</sup>). Thus, 5-MeO-DMT constrains the global structure of neural dynamics.

## **Relationship to experience**

To relate these changes to subjective experience, we fit multilinear regression models employing dominance analysis, exploiting our multiple perspectives on brain dynamics while accounting for predictor-predictor interactions and maintaining interpretability. We do so using alterations in our key analytic measures ( $\Phi$  and H for slow and ultra-slow waves,  $PC_1$  eigenvalue,  $\lambda_{max}$ , intrinsic timescale, and  $E_{MSD=5}$ ) as predictors for self-report scores from 25 custom visual analog scale (VAS) items

# **Article**



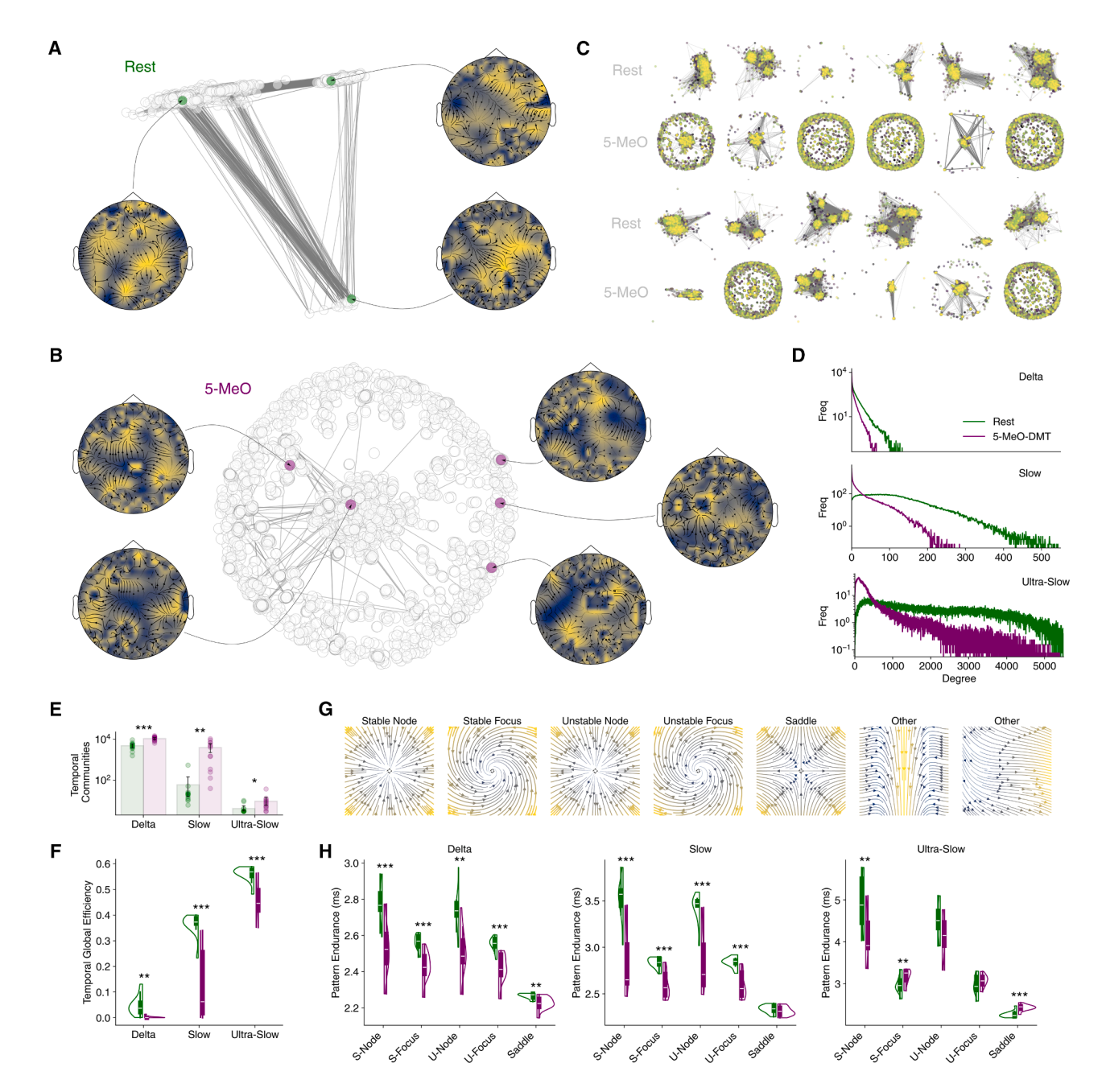


Figure 3. 5-MeO-DMT dampens low-frequency field recurrence and pattern endurance

(A) Field recurrence network with example velocity fields from mode 2 in the rest condition over 15 s of a representative participant. Plotted with communities determined by greedy modularity maximization (25 modules).

- (B) Field recurrence network plot with same parameters for 5-MeO-DMT (1,513 modules).
- (C) Field recurrence network with same parameters for remaining participants.
- (D) Mean histograms for degree distribution of field recurrence networks for each mode.
- (E) Number of communities in recurrence networks for each mode (mean ± SEM).
- (F) Global efficiency for recurrence networks for each mode.
- (G) Illustrations of canonical singularity patterns.
- (H) Average persistence of a flow pattern in the brain. S indicates a stable singularity, and U indicates unstable. Sources (U-Nodes), sinks (S-Nodes), spiral out (U-Focus), spiral in (S-Focus), and saddles.
- (\*p < 0.05, \*\*p < 0.01, and \*\*\*p < 0.001, FDR-corrected Benjamini-Hochberg procedure.



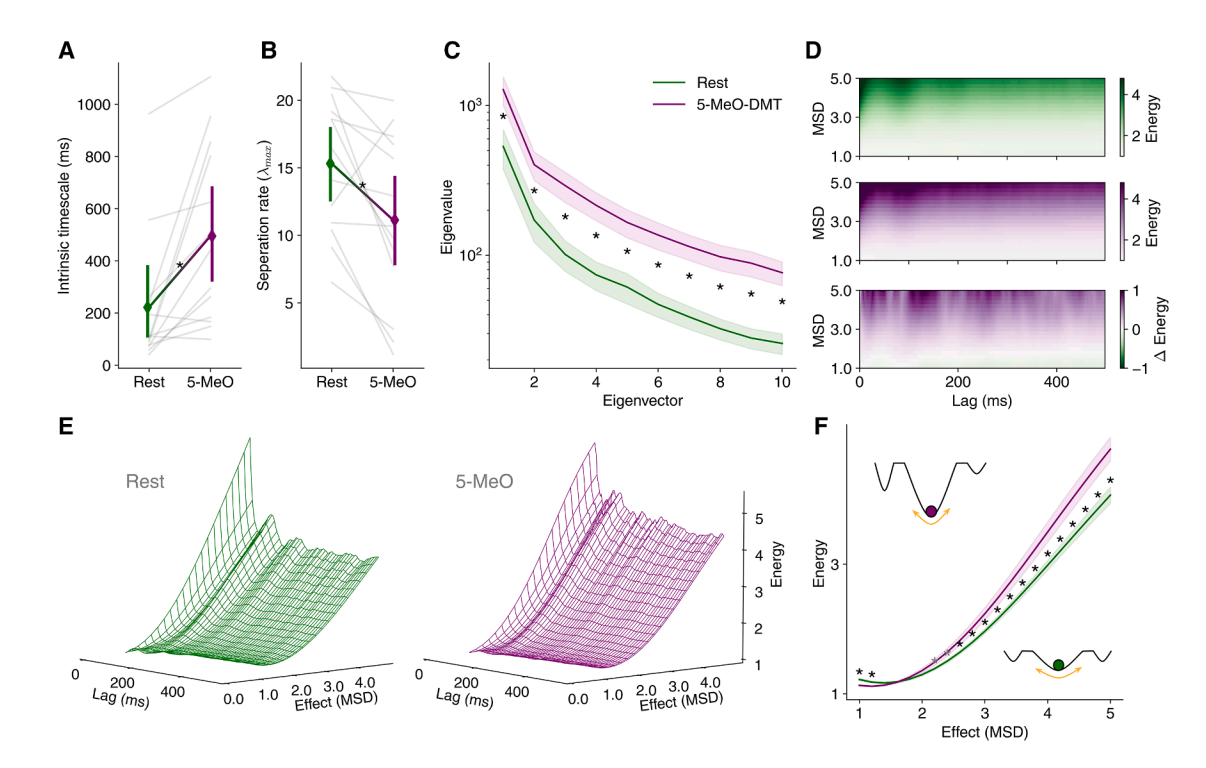


Figure 4. 5-MeO-DMT pushes cortical dynamics toward a low-dimensional steady-state

- (A) Mean decay time of automutual information (AMI) function on broadband signals (mean 95% CI).
- (B) Average separation rate of neighboring points in the phase space of broadband signals (mean 95% CI).
- (C) Eigenvalues for the first 10 eigenvectors from PCA of broadband signals (mean ± SEM).
- (D) 2D average energy landscape for rest (top), 5-MeO-DMT (middle), and their difference (bottom).
- (E) 3D average energy landscape for rest (left) and 5-MeO-DMT (right).
- (F) Energy required for each MSD bin averaged across all lags (mean ± SEM). "Energy well" illustrations are included to depict energetic costs. \*p < 0.05, FDR corrected.

(Figure S12). We find that lifetime 5-MeO-DMT usage is not strongly predicted by our neural measures ( $R^2 = .0372$  and p = 0.306), meaning prior use of the drug likely does not significantly affect brain responses. Next, we find a close fit between changes in brain dynamics and aspects of subjective experience, with the top 5 VAS items obtaining an  $R^2 > 0.7$ , including items such as "unable to lateralize bodily sensations" (p = 0.005), "experienced sense of void" (p = 0.023), "body felt not my own" (p = 0.032), and "experience felt not happening to me" (p = 0.043). However, these p values do not survive false discovery rate (FDR) correction. Importantly, we find that the highest contributing factor to these top predictions was the heterogeneity of ultra-slow wave fields, with the exception of "experienced sense of void" for which the highest was the separation rate ( $\lambda_{max}$ ).

#### **DISCUSSION**

We demonstrate that 5-MeO-DMT, a short-acting psychedelic drug, produces a unique state in the human brain. This state is marked by amplified diffuse slow rhythmic activity that coalesces into spatiotemporally disorganized and dismantled wave patterns unable to travel up and down the putative cortical hierarchy. Furthermore, we find that this disruption pushes

broadband neural activity toward a low-dimensional steady state, paralleling the subjective quality of the experience.

Our results undermine the hypothesis that the induction of diffuse high-amplitude slow oscillations is a universal signature of loss of consciousness. They do, however, provide evidence that augmented low-frequency oscillations are related to environmental disconnection, where subjective experience becomes independent of sensory variables imported from the external world. 55,74–76 This result therefore reinforces the need for establishing more robust neuroscientific methods for discriminating conscious states. We offer the theoretical and empirical contribution that a fruitful strategy will be found by moving beyond one-size-fits-all univariate metrics, such as oscillatory power, toward comprehensive frameworks that permit the detailed characterization of complex spatiotemporal activity

By tracking the extended spatiotemporal patterns of low-frequency flows of neural activity, we discovered crucial characteristics of the 5-MeO-DMT brain state that distinguish it from states of unconsciousness. Rather than triggering simple, coherent, fluid, persistent, recurrent propagating global waves like in anesthesia, <sup>26,28,49</sup> we found that 5-MeO-DMT induces complex, incoherent, viscous, fleeting, unique wave patterns. While these diverse local flows constrain cortex-wide

# **Article**



propagation, it may be the case that they enhance a form of regional collision-based distributed dynamical computation. The 5-MeO-DMT state may therefore be marked by enhanced parallel, but not necessarily integrated, information processing. Future work should investigate how spatiotemporal flow structures relate to taxonomies of multivariate information dynamics, including measures of information transfer and integration. The state of the case that they are the state of the case that they enhance a form of regions and the state of the case that they are the state of the case that they enhance a form of regions and the state of the case that they enhance a form of regions and the state of the case that they enhance a form of regions and the state of the case that they enhance a form of the state of the case that they enhance a form of the state of the case that they enhance a form of the state of the state of the case that they enhance a form of the state of the state of the case that they enhance a form of the state of the s

We found that 5-MeO-DMT instigates more stable low-dimensional broadband behavior with a decreased likelihood of major rapid global activity reconfiguration. These results are consistent with work in mice showing that cortical dynamics become less chaotic under 5-MeO-DMT.<sup>21</sup> This overall simplicity may reasonably occur as a consequence of, rather than in spite of, the complexity seen in low-frequency flows. The lack of collective spatiotemporal coordination of the low-frequency flow fields implies that cortical dynamics are sub-served by a more fragmented network architecture that hinders the recruitment of multiple regions to effectively orchestrate simultaneous large global amplitude deviations. In short, segregation across spatiotemporal scales occurs, deconstructing the brain's canonical functional organization.

Our results contest a number of key concepts in the developing literature on the neuroscience of serotonergic psychedelic drugs. First, whole-brain suppression of alpha power is considered a central feature of the psychedelic state.<sup>78</sup> However, we found that alpha oscillations are not robustly reduced across every part of the cortex, with no deflation in the average oscillatory peak and only right parietal-occipital electrodes reaching significance for reductions in power. Future studies should investigate how alterations in properties such as waveform shape and rhythmicity may be key. Second, psychedelics are thought to "liberate" the bottom-up flow of information via feedforward neural activity. 79,80 In contrast, we found a striking reduction in the probability that low-frequency waves flow in the anterior direction as well as the posterior direction. However. we note that the equivalence between anterior-flowing waves and feedforward processing is overly simplistic. Finally, psychedelics are thought to reduce the curvature of the energy landscape constraining neural activity, allowing more facile activity shifts and higher-dimensional dynamics. 79,81-83 Yet, we found that 5-MeO-DMT steepened the brain's energy landscape, increasing the barriers for major rapid activity shifts and diminishing the dimensionality of neural dynamics. Our results therefore suggest that 5-MeO-DMT has a unique effect on the human brain compared to other classic tryptamine psychedelics.

It is often stated that the unique effects of 5-MeO-DMT, compared to other serotonergic psychedelics, can be accounted for privileged binding to 5-HT<sub>1a</sub> over 5-HT<sub>2a</sub> receptors. <sup>84–87</sup> Such an explanation is appealing to the present study given that the  $G_{\beta\gamma}$  subunit of 5-HT<sub>1a</sub> can activate G-protein-coupled inwardly rectifying potassium channels, causing hyperpolarization, <sup>88</sup> potentially contributing to low-frequency oscillations. It has been shown that HTR2A-knockout (KO) mice, when administered 5-MeO-DMT, exhibit augmented low-frequency oscillations in primary visual cortex that are blocked by a 5-HT<sub>1a</sub> antagonist <sup>89</sup>; however, in a more recent study with wild-type mice, co-administration of 5-MeO-DMT with a 5-HT<sub>1a</sub> antagonist actually further

increased slow-wave activity.90 Nonetheless, if one is committed to a story based on 5-HT<sub>1a</sub>, one would need to explain why other psychedelic drugs, including tryptamines, such as diisopropyltryptamine (DiPT), and phenethylamines, such as mescaline, 3,4methylenedioxyamphetamine (MDA), or 3,4,5-trimethoxamphetamine (TMA), also exhibit such a preference in binding 91,92 while inducing experiences unlike 5-MeO-DMT at high doses. Crucial to this is the fact that binding constants are distinct and dissociable from signaling potency and efficacy, that is to say, between physical association at a receptor and the ability to initiate downstream effects. Recent work has shown that 5-MeO-DMT, like the classical psychedelic lysergic acid diethylamide (LSD), exhibits equipotency at 5-HT<sub>1a</sub> and 5-HT<sub>2a</sub>.93 Moreover, to take the logic from Dourron et al. of a 5-HT<sub>1a</sub>/5-HT<sub>2a</sub> ratio, 85 but here in terms of efficacy at their canonical G-proteins, 5-MeO-DMT would be considered less favoring of 5-HT<sub>1a</sub> over 5-HT<sub>2a</sub> than DMT is (1.2 vs. 1.4).93 In sum, the unique neuropsychopharmacology of 5-MeO-DMT will resist an explanation that simply pits binding at 5-HT<sub>1a</sub> against 5-HT<sub>2a</sub> but may be found in a more advanced treatment of its functional selectivity and biasing of particular signaling cascades at each receptor.

At the mesoscale, we speculate that our results may represent the consequences of a unique shift in the balance of distinct thalamocortical subsystems. The presence of diffuse high-amplitude slow rhythmic activity, reduced communication through coherence, and an approach toward a low-dimensional steady state suggest a reduction in diffuse coupling in the brain. Non-specifically projecting thalamic structures, such as the mediodorsal and centromedian nuclei, may be relieved of their canonical tonic firing patterns, orchestrating supragranular cortical dynamics and global synchronization patterns. 94,95 Instead, cyclical bursting and quiescence of these nuclei may occur, potentially resulting in functional deafferentation 96,97 and cortical activity to become dominated by the intrinsic slow non-stationary bistability prescribed the anatomy of local cortical circuits. 98-100 However, as internal awareness and arousal are maintained, the level of overall thalamocortical resonance expected by wakefulness is likely maintained. Indeed, the presence of fleeting viscous and heterogeneous local flow hints that there could be markedly greater driving gain by structures with targeted projections, like the pulvinar and ventral lateral nucleus, disrupting local excitation-inhibitory balance and overwhelming wave pattern dynamics. We note that this general hypothesis is distinct from existing corticothalamic models of psychedelic action that posit that there is an indiscriminate reduction in thalamic gating. 1,101

#### Limitations of the study

The study suffers from a small number of participants. A substantial proportion of participants were excluded from the analysis, reflecting our stringent exclusion of potential motion artifacts, a common issue for human neuroimaging studies with psychedelic drugs. Despite this, it remains possible that subtle, unaccounted-for motion artifacts could have an influence on EEG recordings. The control condition is a resting-state baseline rather than a blinded placebo group, meaning that expectancy factors are uncontrolled. A standardized single high dose (12-mg) was administered to each participant, and blood samples were not taken throughout, meaning that inter-individual





differences in pharmacokinetics are likely present. Methodologically, our analyses assume the cortex to be a relatively sparse, flat surface and therefore do not account for the high spatial resolution and convoluted geometry inherent to the human brain. Subsequent studies should therefore investigate 5-MeO-DMT with high-density electrophysiological recordings, effective cortical surface modeling, and novel vector field methods for latent Riemannian manifolds. Lastly, the present work does not integrate neural measures with time-resolved phenomenological data. Accordingly, future work should combine neuroimaging with rigorous and dynamic measures of subjective experience, such that inferences about both can mutually constrain each other.

#### Conclusion

In conclusion, we present a detailed neuroscientific investigation in humans of perhaps the most radically altered state of consciousness known. We report novel changes in the spatio-temporal organization of low-frequency waves across the cortex, revealing a disruption in the congruity of the dynamical processes upon which the rest of cortical activity is built. This work not only underscores the need for a revitalized understanding of the role of slow waves in orchestrating subjective experience but emphasizes the need for more comprehensive spatiotemporal methods in neuroscience to better understand the full diversity of human brain states.

#### **RESOURCE AVAILABILITY**

#### **Lead contact**

Further information and requests for materials and data should be directed to and will be fulfilled by the lead contact, George Blackburne (george. blackburne.18@ucl.ac.uk).

## **Materials availability**

This study did not generate any new materials.

### Data and code availability

- Data reported in this paper will be shared by the lead contact upon reasonable request.
- Code is publicly available at <a href="https://github.com/gblackburne/complex-slow-waves">https://github.com/gblackburne/complex-slow-waves</a>, including a Python library for the data-driven decomposition of complex spatiotemporal flow patterns in electrophysiological recordings.
- Any additional information required to reanalyze the data reported in this
  paper is available from the lead contact upon request.

#### **ACKNOWLEDGMENTS**

We are grateful to Tandava Retreats for their generous support in assisting with the data collection process, specifically Victoria Wueschner and Joel Brierre for their pivotal roles in facilitating the 5-MeO-DMT sessions. Additional thanks go to Luis Fabian Rodriguez, Otto Maier, James Sanders, Milly Sellers, and George Deane for providing support during data collection, as well as Raphaël Millière for help with characterizing the phenomenology of 5-MeO-DMT. We extend our deepest thanks to the courageous participants who volunteered for this study. Lastly, we thank supporters of the crowdfunding campaign for helping to secure the funding required to perform this study. G.B. is supported by the Leverhulme Trust. R.G.M. is supported by the Wellcome Trust. J.I.S. is supported by Wellcome Leap.

#### **AUTHOR CONTRIBUTIONS**

Conceptualization, G.B. and R.G.M.; investigation, G.B. and R.G.M.; methodology, G.B. and M.F.; software, G.B. and M.F.; data curation, G.B.; formal analysis, G.B.; project administration, G.B. and R.G.M.; writing – original draft, G.B. and M.F.; writing – review & editing, R.G.M., A.L., S.K.K., P.A.M.M., and J.I.S.; resources, S.K.K.; supervision, S.K.K., P.A.M.M., and J.I.S.

#### **DECLARATION OF INTERESTS**

The authors declare no competing interests.

#### **STAR**\*METHODS

Detailed methods are provided in the online version of this paper and include the following:

- KEY RESOURCES TABLE
- EXPERIMENTAL MODEL AND SUBJECT DETAILS
  - o Ethical statement
  - o Participants
  - Experimental procedures
- METHOD DETAILS
  - EEG preprocessing
  - Empirical mode decomposition
  - o Velocity fields
  - Synchrony
  - o Normalised velocity
  - Heterogeneity
  - o Complex wave patterns
  - o Velocity field recurrence
  - o Recurrence network topology
  - o Intrinsic timescales
  - Separation rate
  - Energy landscape
- QUANTIFICATION AND STATISTICAL ANALYSIS

## SUPPLEMENTAL INFORMATION

Supplemental information can be found online at https://doi.org/10.1016/j.celrep.2025.116040.

Received: January 26, 2025 Revised: April 15, 2025 Accepted: July 2, 2025 Published: July 22, 2025

#### REFERENCES

- Vollenweider, F.X., and Preller, K.H. (2020). Psychedelic drugs: neurobiology and potential for treatment of psychiatric disorders. Nat. Rev. Neurosci. 21, 611–624.
- 2. Nichols, D.E. (2016). Psychedelics. Pharmacol. Rev. 68, 264-355.
- Aday, J.S., Mitzkovitz, C.M., Bloesch, E.K., Davoli, C.C., and Davis, A.K. (2020). Long-term effects of psychedelic drugs: A systematic review. Neurosci. Biobehav. Rev. 113, 179–189.
- Nutt, D., Erritzoe, D., and Carhart-Harris, R. (2020). Psychedelic Psychiatry's Brave New World. Cell 181, 24–28.
- Davis, A.K., Barsuglia, J.P., Lancelotta, R., Grant, R.M., and Renn, E. (2018). The epidemiology of 5-methoxy-N,N-dimethyltryptamine (5-MeO-DMT) use: Benefits, consequences, patterns of use, subjective effects, and reasons for consumption. J. Psychopharmacol. 32, 779–792.
- (2022). European Union Clinical Trials Register. https://www.clinicaltrials register.eu/ctr-search/trial/2022-000574-26/IE.

# **Article**



- (2023). US National Library of Medicine. https://clinicaltrials.gov/study/ NCT05660642.
- 8. (2022). European Union Clinical Trials Register. https://www.clinicaltrialsregister.eu/ctr-search/trial/2021-006861-39/NL.
- (2023). US National Library of Medicine https://clinicaltrials.gov/study/ NCT05674929.
- Miller, M.J., Albarracin-Jordan, J., Moore, C., and Capriles, J.M. (2019). Chemical evidence for the use of multiple psychotropic plants in a 1,000-year-old ritual bundle from South America. Proc. Natl. Acad. Sci. USA 116, 11207–11212.
- 11. Torres, C.M., and Repke, D.B. (2006). Anadenanthera: Visionary Plant of Ancient South America (Routledge).
- Most, A. (1983). Bufo Alvarius: the Psychedelic Toad of the Sonoran Desert.
- 13. Shulgin, A., and Shulgin, A. (1997). TiHKAL: Tryptamines I Have Known and Loved (Transform Press).
- 14. Metzner, R. (2022). The Toad and the Jaguar: A Field Report of Underground Research on a Visionary Medicine Bufo Alvarius and 5-Methoxy-Dimethyltryptamine (Four Trees Press).
- 15. Milliere, R. (2020). The varieties of selflessness. PhiMiSci 1, 1-41.
- Mckilliam, A.K. (2020). What is a global state of consciousness? Phi-MiSci 1.
- Bayne, T., Hohwy, J., and Owen, A.M. (2016). Are There Levels of Consciousness? Trends Cogn. Sci. 20, 405–413.
- Riga, M.S., Lladó-Pelfort, L., Artigas, F., and Celada, P. (2018). The serotonin hallucinogen 5-MeO-DMT alters cortico-thalamic activity in freely moving mice: Regionally-selective involvement of 5-HT1A and 5-HT2A receptors. Neuropharmacology 142, 219–230.
- Souza, A.C., Souza, B.C., França, A., Moradi, M., Souza, N.C., Leão, K. E., Tort, A.B.L., Leão, R.N., Lopes-Dos-Santos, V., and Ribeiro, S. (2024).
   MeO-DMT induces sleep-like LFP spectral signatures in the hippocampus and prefrontal cortex of awake rats. Sci. Rep. 14, 11281.
- Bréant, B.J.B., Mengual, J.P., Bannerman, D.M., Sharp, T., and Vyazovskiy, V.V. (2022). "Paradoxical wakefulness" induced by psychedelic 5-methoxy-N,N-dimethyltryptamine in mice. Preprint at bioRxiv.
- Toker, D., Müller, E., Miyamoto, H., Riga, M.S., Lladó-Pelfort, L., Yamakawa, K., Artigas, F., Shine, J.M., Hudson, A.E., Pouratian, N., and Monti, M.M. (2024). Criticality supports cross-frequency cortical-thalamic information transfer during conscious states. eLife 13, e86547.
- Ní Mhuircheartaigh, R., Warnaby, C., Rogers, R., Jbabdi, S., and Tracey, I. (2013). Slow-wave activity saturation and thalamocortical isolation during propofol anesthesia in humans. Sci. Transl. Med. 5, 208ra148.
- Schiff, N.D., Nauvel, T., and Victor, J.D. (2014). Large-scale brain dynamics in disorders of consciousness. Curr. Opin. Neurobiol. 25, 7–14.
- 24. Rosanova, M., Fecchio, M., Casarotto, S., Sarasso, S., Casali, A.G., Pigorini, A., Comanducci, A., Seregni, F., Devalle, G., Citerio, G., et al. (2018). Sleep-like cortical OFF-periods disrupt causality and complexity in the brain of unresponsive wakefulness syndrome patients. Nat. Commun. 9, 4427.
- Frohlich, J., Mediano, P.A.M., Bavato, F., and Gharabaghi, A. (2023). Paradoxical pharmacological dissociations result from drugs that enhance delta oscillations but preserve consciousness. Commun. Biol. 6, 654.
- Bhattacharya, S., Donoghue, J.A., Mahnke, M., Brincat, S.L., Brown, E. N., and Miller, E.K. (2022). Propofol Anesthesia Alters Cortical Traveling Waves. J. Cogn. Neurosci. 34, 1274–1286.
- Massimini, M., Huber, R., Ferrarelli, F., Hill, S., and Tononi, G. (2004). The sleep slow oscillation as a traveling wave. J. Neurosci. 24, 6862–6870.
- 28. Fabus, M.S., Woolrich, M.W., and Warnaby, C.E. (2022). Brainwave viscosity in propofol anaesthesia. Br. J. Anaesth. *128*, e61–e62.
- Siclari, F., Bernardi, G., Riedner, B.A., LaRocque, J.J., Benca, R.M., and Tononi, G. (2014). Two distinct synchronization processes in the transi-

- tion to sleep: a high-density electroencephalographic study. Sleep 37, 1621–1637
- Foster, M., and Scheinost, D. (2024). Brain states as wave-like motifs. Trends Cogn. Sci. 28, 492–503.
- Roberts, J.A., Gollo, L.L., Abeysuriya, R.G., Roberts, G., Mitchell, P.B., Woolrich, M.W., and Breakspear, M. (2019). Metastable brain waves. Nat. Commun. 10, 1056.
- 32. Pang, J.C., Aquino, K.M., Oldehinkel, M., Robinson, P.A., Fulcher, B.D., Breakspear, M., and Fornito, A. (2023). Geometric constraints on human brain function. Nature *618*, 566–574.
- **33.** Kampis, G. (1991). Self-Modifying Systems in Biology and Cognitive Science (Pergamon Press).
- 34. Maturana, H.R., and Varela, F.J. (1972). On Machines and Living Beings (Editorial Universitaria).
- **35.** Adrian, E.D., and Matthews, B.H. (1934). The interpretation of potential waves in the cortex. J. Physiol. *81*, 440–471.
- Mohajerani, M.H., Chan, A.W., Mohsenvand, M., LeDue, J., Liu, R., McVea, D.A., Boyd, J.D., Wang, Y.T., Reimers, M., and Murphy, T.H. (2013). Spontaneous cortical activity alternates between motifs defined by regional axonal projections. Nat. Neurosci. 16, 1426–1435.
- Townsend, R.G., Solomon, S.S., Chen, S.C., Pietersen, A.N.J., Martin, P. R., Solomon, S.G., and Gong, P. (2015). Emergence of complex wave patterns in primate cerebral cortex. J. Neurosci. 35, 4657–4662.
- Rubino, D., Robbins, K.A., and Hatsopoulos, N.G. (2006). Propagating waves mediate information transfer in the motor cortex. Nat. Neurosci. 9, 1549–1557.
- Huang, X., Xu, W., Liang, J., Takagaki, K., Gao, X., and Wu, J.Y. (2010).
   Spiral wave dynamics in neocortex. Neuron 68, 978–990.
- Xu, Y., Long, X., Feng, J., and Gong, P. (2023). Interacting spiral wave patterns underlie complex brain dynamics and are related to cognitive processing. Nat. Hum. Behav. 7, 1196–1215.
- Gong, P., and van Leeuwen, C. (2009). Distributed dynamical computation in neural circuits with propagating coherent activity patterns. PLoS Comput. Biol. 5, e1000611.
- Chen, G., and Gong, P. (2019). Computing by modulating spontaneous cortical activity patterns as a mechanism of active visual processing. Nat. Commun. 10, 4915.
- Heitmann, S., Rule, M., Truccolo, W., and Ermentrout, B. (2017). Optogenetic Stimulation Shifts the Excitability of Cerebral Cortex from Type I to Type II: Oscillation Onset and Wave Propagation. PLoS Comput. Biol. 13, e1005349.
- 44. Pinotsis, D.A., and Miller, E.K. (2023). In vivo ephaptic coupling allows memory network formation. Cereb. Cortex 33, 9877–9895.
- Das, A., Zabeh, E., Ermentrout, B., and Jacobs, J. (2024). Planar, Spiral, and Concentric Traveling Waves Distinguish Cognitive States in Human Memory. Preprint at bioRxiv. https://doi.org/10.1101/2024.01.26. 577456.
- Muller, L., Reynaud, A., Chavane, F., and Destexhe, A. (2014). The stimulus-evoked population response in visual cortex of awake monkey is a propagating wave. Nat. Commun. 5, 3675.
- 47. Lee, S.-H., Blake, R., and Heeger, D.J. (2005). Traveling waves of activity in primary visual cortex during binocular rivalry. Nat. Neurosci. 8, 22–23.
- Davis, Z.W., Muller, L., Martinez-Trujillo, J., Sejnowski, T., and Reynolds, J.H. (2020). Spontaneous travelling cortical waves gate perception in behaving primates. Nature 587, 432–436.
- Liang, Y., Liang, J., Song, C., Liu, M., Knöpfel, T., Gong, P., and Zhou, C. (2023). Complexity of cortical wave patterns of the wake mouse cortex. Nat. Commun. 14, 1434.
- Munn, B.R., Müller, E.J., Wainstein, G., and Shine, J.M. (2021). The ascending arousal system shapes neural dynamics to mediate awareness of cognitive states. Nat. Commun. 12, 6016.





- Skarda, C.A., and Freeman, W.J. (1987). How brains make chaos in order to make sense of the world. Behav. Brain Sci. 10. 161–173.
- 52. Valle, M., Maqueda, A.E., Rabella, M., Rodríguez-Pujadas, A., Antonijoan, R.M., Romero, S., Alonso, J.F., Mañanas, M.À., Barker, S., Friedlander, P., et al. (2016). Inhibition of alpha oscillations through serotonin-2A receptor activation underlies the visual effects of ayahuasca in humans. Eur. Neuropsychopharmacol. 26, 1161–1175.
- Pallavicini, C., Cavanna, F., Zamberlan, F., de la Fuente, L.A., Ilksoy, Y., Perl, Y.S., Arias, M., Romero, C., Carhart-Harris, R., Timmermann, C., and Tagliazucchi, E. (2021). Neural and subjective effects of inhaled N, N-dimethyltryptamine in natural settings. J. Psychopharmacol. 35, 406–420.
- Pallavicini, C., Vilas, M.G., Villarreal, M., Zamberlan, F., Muthukumaraswamy, S., Nutt, D., Carhart-Harris, R., and Tagliazucchi, E. (2019). Spectral signatures of serotonergic psychedelics and glutamatergic dissociatives. Neuroimage 200, 281–291.
- Timmermann, C., Roseman, L., Schartner, M., Milliere, R., Williams, L.T. J., Erritzoe, D., Muthukumaraswamy, S., Ashton, M., Bendrioua, A., Kaur, O., et al. (2019). Neural correlates of the DMT experience assessed with multivariate EEG. Sci. Rep. 9, 16324.
- Timmermann, C., Roseman, L., Haridas, S., Rosas, F.E., Luan, L., Kettner, H., Martell, J., Erritzoe, D., Tagliazucchi, E., Pallavicini, C., et al. (2023). Human brain effects of DMT assessed via EEG-fMRI. Proc. Natl. Acad. Sci. USA 120, e2218949120.
- Muthukumaraswamy, S.D., Carhart-Harris, R.L., Moran, R.J., Brookes, M.J., Williams, T.M., Errtizoe, D., Sessa, B., Papadopoulos, A., Bolstridge, M., Singh, K.D., et al. (2013). Broadband cortical desynchronization underlies the human psychedelic state. J. Neurosci. 33, 15171– 15183
- Schenberg, E.E., Alexandre, J.F.M., Filev, R., Cravo, A.M., Sato, J.R., Muthukumaraswamy, S.D., Yonamine, M., Waguespack, M., Lomnicka, I., Barker, S.A., and da Silveira, D.X. (2015). Acute Biphasic Effects of Ayahuasca. PLoS One 10, e0137202.
- Carhart-Harris, R.L., Muthukumaraswamy, S., Roseman, L., Kaelen, M., Droog, W., Murphy, K., Tagliazucchi, E., Schenberg, E.E., Nest, T., Orban, C., et al. (2016). Neural correlates of the LSD experience revealed by multimodal neuroimaging. Proc. Natl. Acad. Sci. USA 113, 4853–4858.
- 60. Riba, J., Anderer, P., Morte, A., Urbano, G., Jané, F., Saletu, B., and Barbanoj, M.J. (2002). Topographic pharmaco-EEG mapping of the effects of the South American psychoactive beverage ayahuasca in healthy volunteers. Br. J. Clin. Pharmacol. 53, 613–628.
- 61. Riba, J., Anderer, P., Jané, F., Saletu, B., and Barbanoj, M.J. (2004). Effects of the South American psychoactive beverage ayahuasca on regional brain electrical activity in humans: a functional neuroimaging study using low-resolution electromagnetic tomography. Neuropsychobiology 50, 89–101.
- Don, N.S., McDonough, B.E., Moura, G., Warren, C.A., Kawanishi, K., Tomita, H., Tachibana, Y., Böhlke, M., and Farnsworth, N.R. (1998). Effects of Ayahuasca on the human EEG. Phytomedicine 5, 87–96.
- 63. Ort, A., Smallridge, J.W., Sarasso, S., Casarotto, S., von Rotz, R., Casanova, A., Seifritz, E., Preller, K.H., Tononi, G., and Vollenweider, F.X. (2023). TMS-EEG and resting-state EEG applied to altered states of consciousness: oscillations, complexity, and phenomenology. iScience 26, 106589.
- Barnett, L., Muthukumaraswamy, S.D., Carhart-Harris, R.L., and Seth, A. K. (2020). Decreased directed functional connectivity in the psychedelic state. Neuroimage 209, 116462.
- Kometer, M., Pokorny, T., Seifritz, E., and Volleinweider, F.X. (2015). Psilocybin-induced spiritual experiences and insightfulness are associated with synchronization of neuronal oscillations. Psychopharmacology 232, 3663–3676.

- Van Ede, F., Quinn, A.J., Woolrich, M.W., and Nobre, A.C. (2018). Neural Oscillations: Sustained Rhythms or Transient Burst-Events? Trends Neurosci. 41, 415–417.
- Cole, S.R., and Voytek, B. (2017). Brain Oscillations and the Importance of Waveform Shape. Trends Cogn. Sci. 21, 137–149.
- Uddin, L.Q. (2020). Bring the Noise: Reconceptualizing Spontaneous Neural Activity. Trends Cogn. Sci. 24, 734–746.
- 69. Quinn, A.J., Lopes-Dos-Santos, V., Huang, N., Liang, W.K., Juan, C.H., Yeh, J.R., Nobre, A.C., Dupret, D., and Woolrich, M.W. (2021). Within-cycle instantaneous frequency profiles report oscillatory waveform dynamics. J. Neurophysiol. 126, 1190–1208.
- Hazarika, N., Tsoi, A.C., and Sergejew, A.A. (1997). Nonlinear considerations in EEG signal classification. IEEE Trans. Signal Process. 45, 829–836.
- García-Rosales, F., Schaworonkow, N., and Hechavarria, J.C. (2024).
   Oscillatory Waveform Shape and Temporal Spike Correlations Differ across Bat Frontal and Auditory Cortex. J. Neurosci. 44.
- Donoghue, T., Haller, M., Peterson, E.J., Varma, P., Sebastian, P., Gao, R., Noto, T., Lara, A.H., Wallis, J.D., Knight, R.T., et al. (2020). Parameterizing neural power spectra into periodic and aperiodic components. Nat. Neurosci. 23, 1655–1665.
- Fabus, M.S., Quinn, A.J., Warnaby, C.E., and Woolrich, M.W. (2021).
   Automatic decomposition of electrophysiological data into distinct non-sinusoidal oscillatory modes. J. Neurophysiol. 126, 1670–1684.
- Martial, C., Piarulli, A., Gosseries, O., Cassol, H., Ledoux, D., Charland-Verville, V., and Laureys, S. (2024). EEG signature of near-death-like experiences during syncope-induced periods of unresponsiveness. Neuroimage 298, 120759.
- Vesuna, S., Kauvar, I.V., Richman, E., Gore, F., Oskotsky, T., Sava-Segal, C., Luo, L., Malenka, R.C., Henderson, J.M., Nuyujukian, P., et al. (2020).
   Deep posteromedial cortical rhythm in dissociation. Nature 586, 87–94.
- Acosta-Urquidi, J. (2015). QEEG Studies of the Acute Effects of the Visionary Tryptamine DMT. Cosmos Hist. J. Nat. Soc. Philos. 11, 115–129.
- Mediano, P.A.M., Rosas, F.E., Luppi, A.I., Carhart-Harris, R.L., Bor, D., Seth, A.K., and Barrett, A.B. (2021). Towards an extended taxonomy of information dynamics via Integrated Information Decomposition. Preprint at arXiv. https://doi.org/10.48550/arXiv.2109.13186.
- Erritzoe, D., Timmermann, C., Godfrey, K., Castro-Rodrigues, P., Peill, J., Carhart-Harris, R.L., Nutt, D.J., and Wall, M.B. (2024). Exploring mechanisms of psychedelic action using neuroimaging. Nat. Ment. Health 2, 141–153.
- Carhart-Harris, R.L., and Friston, K.J. (2019). REBUS and the Anarchic Brain: Toward a Unified Model of the Brain Action of Psychedelics. Pharmacol. Rev. 71, 316–344.
- Alamia, A., Timmermann, C., Nutt, D.J., VanRullen, R., and Carhart-Harris, R.L. (2020). DMT alters cortical travelling waves. eLife 9, e59784.
- Hipólito, I., Mago, J., Rosas, F.E., and Carhart-Harris, R. (2023). Pattern breaking: a complex systems approach to psychedelic medicine. Neurosci. Conscious. 2023, niad017.
- 82. Girn, M., Rosas, F.E., Daws, R.E., Gallen, C.L., Gazzaley, A., and Carhart-Harris, R.L. (2023). A complex systems perspective on psychedelic brain action. Trends Cogn. Sci. 27, 433–445.
- Singleton, S.P., Luppi, A.I., Carhart-Harris, R.L., Cruzat, J., Roseman, L., Nutt, D.J., Deco, G., Kringelbach, M.L., Stamatakis, E.A., and Kuceyeski, A. (2022). Receptor-informed network control theory links LSD and psilocybin to a flattening of the brain's control energy landscape. Nat. Commun. 13, 5812.
- 84. Reckweg, J.T., Uthaug, M.V., Szabo, A., Davis, A.K., Lancelotta, R., Mason, N.L., and Ramaekers, J.G. (2022). The clinical pharmacology and potential therapeutic applications of 5-methoxy-N,N-dimethyltryptamine (5-MeO-DMT). J. Neurochem. 162, 128–146.

## **Article**



- Dourron, H.M., Nichols, C.D., Simonsson, O., Bradley, M., Carhart-Harris, R., and Hendricks, P.S. (2023). 5-MeO-DMT: An atypical psychedelic with unique pharmacology, phenomenology & risk? Psychopharmacology 242, 1457–1479.
- Ermakova, A.O., Dunbar, F., Rucker, J., and Johnson, M.W. (2022). A narrative synthesis of research with 5-MeO-DMT. J. Psychopharmacol. 36, 273–294.
- Jefferson, S.J., Gregg, I., Dibbs, M., Liao, C., Wu, H., Davoudian, P.A., Woodburn, S.C., Wehrle, P.H., Sprouse, J.S., Sherwood, A.M., et al. (2023). 5-MeO-DMT modifies innate behaviors and promotes structural neural plasticity in mice. Neuropsychopharmacology 48, 1257–1266.
- Savalia, N.K., Shao, L.-X., and Kwan, A.C. (2021). A Dendrite-Focused Framework for Understanding the Actions of Ketamine and Psychedelics. Trends Neurosci. 44, 260–275.
- 89. Riga, M.S., Bortolozzi, A., Campa, L., Artigas, F., and Celada, P. (2016). The serotonergic hallucinogen 5-methoxy-N,N-dimethyltryptamine disrupts cortical activity in a regionally-selective manner via 5-HT(1A) and 5-HT(2A) receptors. Neuropharmacology 101, 370–378.
- Bréant, B.J.B., Mengual, J.P., Bannerman, D.M., Sharp, T., and Vyazovskiy, V.V. (2024). Sleep-like state during wakefulness induced by psychedelic 5-MeO-DMT in mice. Preprint at bioRxiv. https://doi.org/10.1101/ 2022.12.11.519886.
- Ray, T.S. (2010). Psychedelics and the human receptorome. PLoS One 5, e9019.
- Besnard, J., Ruda, G.F., Setola, V., Abecassis, K., Rodriguiz, R.M., Huang, X.P., Norval, S., Sassano, M.F., Shin, A.I., Webster, L.A., et al. (2012). Automated design of ligands to polypharmacological profiles. Nature 492, 215–220.
- Warren, A.L., Lankri, D., Cunningham, M.J., Serrano, I.C., Parise, L.F., Kruegel, A.C., Duggan, P., Zilberg, G., Capper, M.J., Havel, V., et al. (2024). Structural pharmacology and therapeutic potential of 5-methoxytryptamines. Nature 630, 237–246.
- Shine, J.M. (2021). The thalamus integrates the macrosystems of the brain to facilitate complex, adaptive brain network dynamics. Prog. Neurobiol. 199, 101951.
- Shine, J.M., Lewis, L.D., Garrett, D.D., and Hwang, K. (2023). The impact of the human thalamus on brain-wide information processing. Nat. Rev. Neurosci. 24, 416–430.
- Llinás, R.R., and Steriade, M. (2006). Bursting of thalamic neurons and states of vigilance. J. Neurophysiol. 95, 3297–3308.
- 97. Neske, G.T. (2015). The slow oscillation in cortical and thalamic networks: Mechanisms and functions. Front. Neural Circ. 9, 88.
- 98. Sanchez-Vives, M.V., and Mattia, M. (2014). Slow wave activity as the default mode of the cerebral cortex. Arch. Ital. Biol. *152*, 147–155.
- Sanchez-Vives, M.V., Massimini, M., and Mattia, M. (2017). Shaping the Default Activity Pattern of the Cortical Network. Neuron 94, 993–1001.
- Sanchez-Vives, M.V., and McCormick, D.A. (2000). Cellular and network mechanisms of rhythmic recurrent activity in neocortex. Nat. Neurosci. 3, 1027–1034.
- Vollenweider, F.X., and Geyer, M.A. (2001). A systems model of altered consciousness: integrating natural and drug-induced psychoses. Brain Res. Bull. 56, 495–507.
- 102. Gramfort, A., Luessi, M., Larson, E., Engemann, D.A., Strohmeier, D., Brodbeck, C., Parkkonen, L., and Hämäläinen, M.S. (2014). MNE software for processing MEG and EEG data. Neuroimage 86, 446–460.
- 103. Tenke, C.E., and Kayser, J. (2001). A convenient method for detecting electrolyte bridges in multichannel electroencephalogram and eventrelated potential recordings. Clin. Neurophysiol. 112, 545–550.
- 104. Greischar, L.L., Burghy, C.A., van Reekum, C.M., Jackson, D.C., Pizzagalli, D.A., Mueller, C., and Davidson, R.J. (2004). Effects of electrode density and electrolyte spreading in dense array electroencephalographic recording. Clin. Neurophysiol. 115, 710–720.

- 105. Fabus, M.S., Woolrich, M.W., Warnaby, C.W., and Quinn, A.J. (2022). Understanding Harmonic Structures Through Instantaneous Frequency. IEEE Open J. Signal Process. 3, 320–334.
- 106. Huang, N.E., Shen, Z., Long, S.R., Wu, M.C., Shih, H.H., Zheng, Q., Yen, N.C., Tung, C.C., and Liu, H.H. (1998). The empirical mode decomposition and the Hilbert spectrum for nonlinear and non-stationary time series analysis. Proc. R. Soc. A 454, 903–995.
- Yang, Y., Deng, J., and Wu, C. (2009). Analysis of Mode Mixing Phenomenon in the Empirical Mode Decomposition Method. In 2009 Second International Symposium on Information Science and Engineering (IEEE), pp. 553–556.
- Bueno-López, M., Giraldo, E., Molinas, M., and Fosso, O. (2019). The Mode Mixing Problem and its Influence in the Neural Activity Reconstruction. IAENG Int. J. Comput. Sci. 46, 11.
- Huang, N.E. (2014). Hilbert-huang Transform and its Applications (World Scientific).
- 110. Huang, N.E., Hu, K., Yang, A.C.C., Chang, H.C., Jia, D., Liang, W.K., Yeh, J.R., Kao, C.L., Juan, C.H., Peng, C.K., et al. (2016). On Holo-Hilbert spectral analysis: a full informational spectral representation for nonlinear and non-stationary data. Philos. Trans. A Math. Phys. Eng. Sci. 374, 20150206.
- 111. Quinn, A.J., Lopes-Dos-Santos, V., Dupret, D., Nobre, A.C., and Woolrich, M.W. (2021). EMD: Empirical Mode Decomposition and Hilbert-Huang Spectral Analyses in Python. J. Open Source Softw. 6, 2977.
- Hussain, A.K.M.F. (1986). Coherent structures and turbulence. J. Fluid Mech. 173, 303–356.
- Horn, B.K.P., and Schunck, B.G. (1981). Determining optical flow. Artif. Intell. 17, 185–203.
- Wildie, M., and Shanahan, M. (2012). Metastability and chimera states in modular delay and pulse-coupled oscillator networks. Chaos 22, 043131.
- Shanahan, M. (2010). Metastable chimera states in community-structured oscillator networks. Chaos 20, 013108.
- Vicsek, T., and Zafeiris, A. (2012). Collective motion. Phys. Rep. 517, 71–140.
- 117. Perry, A.E., and Chong, M.S. (1987). A description of eddying motions and flow patterns using critical-point concepts. Annu. Rev. Fluid Mech. 19, 125–155.
- 118. Varley, T.F., and Sporns, O. (2021). Network analysis of time series: Novel approaches to network neuroscience. Front. Neurosci. 15, 787068.
- Clauset, A., Newman, M.E.J., and Moore, C. (2004). Finding community structure in very large networks. Phys. Rev. E Stat. Nonlin. Soft Matter Phys. 70, 066111.
- Newman, M.E.J. (2016). Equivalence between modularity optimization and maximum likelihood methods for community detection. Phys. Rev. E 94, 052315.
- 121. Sorrentino, P., Rabuffo, G., Baselice, F., Troisi Lopez, E., Liparoti, M., Quarantelli, M., Sorrentino, G., Bernard, C., and Jirsa, V. (2023). Dynamical interactions reconfigure the gradient of cortical timescales. Netw. Neurosci. 7, 73–85.
- Rosenstein, M.T., Collins, J.J., and De Luca, C.J. (1993). A practical method for calculating largest Lyapunov exponents from small data sets. Physica D 65, 117–134.
- 123. Müller, E.J., Munn, B.R., Redinbaugh, M.J., Lizier, J., Breakspear, M., Saalmann, Y.B., and Shine, J.M. (2023). The non-specific matrix thalamus facilitates the cortical information processing modes relevant for conscious awareness. Cell Rep. 42, 112844.
- 124. Taylor, N.L., Whyte, C.J., Munn, B.R., Chang, C., Lizier, J.T., Leopold, D. A., Turchi, J.N., Zaborszky, L., Műller, E.J., and Shine, J.M. (2024). Causal evidence for cholinergic stabilization of attractor landscape dynamics. Cell Rep. 43, 114359.





## **STAR**\*METHODS

#### **KEY RESOURCES TABLE**

REAGENT or RESOURCE	SOURCE	IDENTIFIER
Software and algorithms		
Python		https://www.python.org/
MNE	Gramfort et al. 102	https://mne.tools/
it-EMD	Fabus et al. <sup>73</sup>	https://gitlab.com/emd-dev/emd
Custom code	This paper	https://github.com/gblackburne/complex-slow-waves

#### **EXPERIMENTAL MODEL AND SUBJECT DETAILS**

#### **Ethical statement**

This study was conducted in accordance with the Declaration of Helsinki and approved by the University College London (UCL) Research Ethics Committee (ID: 19437/004). The study was conducted in collaboration with Tandava Retreat Center (TRC), who provided trained facilitators and facilities. All participants provided informed consent via a secure online platform after reviewing comprehensive study information. Participation was voluntary and uncompensated. Participants were informed of their right to withdraw at any stage of the study without penalty and were provided with information about sources of support in case of any distress related to the study.

#### **Participants**

Participants were recruited globally through the study advertisement on the F.I.V.E. (5-MeO-DMT Information & Vital Education) platform (www.five-meo.education), social media, news outlets, and word-of-mouth. Potential participants underwent a four-stage screening process: (1) TRC online screening, (2) TRC facilitator interview, (3) UCL online screening, and (4) UCL researcher interview (RM, GB). Exclusion criteria included: age <18 years, no prior 5-MeO-DMT experience, significant physical illness (e.g., epilepsy, heart disease), psychiatric diagnoses, use of psychiatric medications of any kind, family history of psychosis, history of adverse reactions psychedelic drugs. 5-MeO-DMT is also known to in some individuals promote involuntary bodily movement or seizure-like behavior, <sup>85</sup> as such we specifically recruited participants that have no history of such responses. Eligible participants (*N* = 32) were initially assigned to one of six three-day retreats, with assignments based on availability and balanced distribution. However, three participants withdrew before the retreats began. The final cohort (*N* = 29; 16 male, 13 female; mean age = 48.52 years, SD = 10.44, range = 34–75) was predominantly White/Caucasian (86.21%). The majority of participants held a Bachelor's degree (58.62%) and identified as non-religious (93.10%). Mean lifetime 5-MeO-DMT use was 39.03 occasions (SD = 72.91, range = 1–300). Detailed participant characteristics are provided in Table S1.

#### **Experimental procedures**

The study was conducted in a naturalistic setting, at a retreat center. The study followed a three-day protocol including a preparation day consisting of orientation and participant briefing (Day 1), a dosing day for 5-MeO-DMT administration and primary data collection (Day 2), and an integration day featuring facilitator-guided group discussions (Day 3). This setup was consistent across all six retreats. Participants were instructed to refrain from consuming drugs, with the exception of nicotine containing products, for two weeks prior to dosing. On dosing day, participants fasted and abstained from caffeine. Individual dosing sessions commenced at 08:00 a.m. in 90-min intervals. At all times during every session, two certified professional facilitators were present to ensure participant safety and provide psychological support if necessary. Each session began with a 7-min baseline eye-closed resting-state EEG recorded with participants seated in a self-selected comfortable position conducive to minimal movement. Participants were instructed to remain relaxed but wakeful, and to alert experimenters if they felt like they may fall asleep. Participants then moved to a centrally located padded recliner, where they assumed a semi-supine position equipped with a standardised neck pillow and opaque eye mask. Synthetic 5-MeO-DMT (12 mg) was vaporised using an argon gas piston vaporiser (203°C-210°C, ~ 120s heating). Following a standardised 2-3 min relaxation exercise, participants inhaled the vapor in a single breath and were instructed to maximise breath retention before exhalation, as per protocols established during preparation. EEG recording began at the moment of completed inhalation, and continued for 20 min post-inhalation. Consistent with the resting-state baseline, participants were instructed to keep eyes-closed during the entire recording. The EEG system was a saline-based 64-channel ANT Neuro Waveguard Net connected to an NA-261 EEG amplifier, recorded at 500 Hz, with Ag electrode placement following the 10-20 system (reference: CPz, ground: AFz, impedance <20 k Ω). Ambient non-percussive music was played throughout the baseline and drug period, and a Koshi bell was rung when EEG recording was complete. Post-session, participants rested for a self-determined period after which they completed

# **Cell Reports**Article



questionnaires, including a 25-item custom visual analogue scale for characterising specific self-related alterations in subjective experience (Figure S11), and also had a micro-phenomenological interview.

#### **METHOD DETAILS**

#### **EEG** preprocessing

Preprocessing was performed using custom scripts using MNE-Python. 102 Participants were excluded from analysis if their physiological artifacts (ocular, muscular, respiratory, or cardiovascular) were substantial enough to necessitate the removal of over 50% of the data collected within the first 10 min post-drug administration (10 participants). Data was filtered using a finite impulse response (FIR) one-pass, zero-phase, non-causal bandpass filter at 0.1-50 Hz. Data was segmented into non-overlapping 3s epochs, producing 140 epochs for the baseline condition and 400 epochs for the drug condition. Electrolyte bridging was computed using the intrinsic Hjorth algorithm with a 16  $\mu$ V<sup>2</sup> cut-off. <sup>103,104</sup> Participants with  $\geq$  1% of potential total bridges, or significant bridging that localises such that interpolation would depend on sensors which are also bridged, were excluded from further analysis (1 participant). For those with <1 %, spherical spline interpolation was performed via the generation of virtual channels between bridged electrodes (Rest: 3.684 ± 2.076, 5-MeO-DMT: 1.158 ± 0.785 bridges). Sensor time series were manually inspected to identify bad channels, participants with >20 bad channels were excluded from further analysis (0 participants), and those with <20 bad channels had these interpolated from surrounding sensors (Rest: 7.579 ± 1.049, 5-MeO-DMT: 7.368 ± 1.06 channel). Extended infomax independent components analysis (ICA) was performed with 40 components, and those manually deemed to be equipment noise or physiological artifacts were zeroed out and excluded from sensor signal reconstruction (Rest: 4.842 ± 0.766, 5-MeO-DMT: 5.053 ± 0.89 components). Epochs corrupted by noise or physiological arefacts were manually removed (Rest: 3.611 ± 2.267, 5-MeO-DMT: 38.105 ± 10.718 epochs). Data was baseline corrected and rereferenced to an average reference. This resulted in 19 subjects with epoch data, 13 of which were extremely still such that they had an artifact-free continuous minute at the peak of the drug's effects.

#### **Empirical mode decomposition**

A central challenge in time series analysis is creating robust representations of the frequency content of complex signals. The standard approach in neuroscience for doing so is based on the Fourier Transform (FT). The FT is a powerful and versatile technique that seeks to represent a signal as a combination of strictly linear sinusoidal basis functions. However, brain rhythms are noisy, exhibit distinctly non-sinusoidal waveforms, and enter into transient bursting behavior. 66-71 This presents a challenge for the FT, since it cannot fully and directly represent the non-sinusoidal forms at their intrinsic frequency, instead assuming them to be partly the result of a higher frequency harmonic. This is problematic for neuroscience, since the canonical electrophysiological frequency bands are all harmonics of a lower band, and the power in each specific band is a variable of interest in its own right for distinguishing different brain states. This problem is exacerbated by the fact that brain signals comprise a myriad of multiplexing oscillations, each with their own harmonics. Furthermore, the linear basis functions of the FT are static, meaning that in order to characterise evolving brain activity analysts must use a windowing technique that inherently blurs the ongoing dynamics.

An elegant solution to these problems comes from Empirical Mode Decomposition (EMD), which permits the automatic decomposition of signals into a finite number of distinct dynamic non-linear oscillatory modes, known as Intrinsic Mode Functions (IMFs). <sup>106</sup> EMD sifts the IMFs out of a signal, from fastest to slowest, in an iterative process of peak-trough detection, amplitude envelope interpolation and subtraction. Here, we use the recently developed iterated-masking EMD (itEMD), as it has been shown to be an automated solution to the mode mixing problem. <sup>73,107,108</sup>

We then compute the instantaneous phase, frequency and amplitude of each IMF via the Normalized Hilbert-Huang transform (HHT), 109,110 with the signal's time-resolved power spectrum being an instantaneous amplitude weighted representation of frequency content. 111

Finally, to investigate the specific frequency content of amplitude modulations in our signals, we perform a second level sift on the instantaneous amplitudes of each IMF, producing a set of higher-order IMFs which represent the frequency content (amplitude modulation frequency) of dynamical changes in oscillatory power (carrier frequency). Carrier frequencies are placed into 50 linearly spaced histogram bins 0.5-4Hz and amplitude-modulation frequencies are placed into 50 linearly spaced bins 8-50Hz, producing the holospectrum.

#### **Velocity fields**

Velocity vector fields are mathematical tools from physical theories of fluid dynamics that include descriptions of vortices and eddies in collective fluid motion. Recently, velocity fields have been appropriated in neuroscience to characterise the structure of large-scale propagating patterns of neural activity, adapting techniques from optical flow estimation in computer science. 77,113

First, the instantaneous amplitude of an IMF is pushed onto a 32x32 scalp grid, using radial basis function interpolation and a multidimensional Gaussian kernel of width 1 S.D, creating the sequence  $\phi(x,y,t)$ . The velocity field  $\mathbf{v}_{\phi}(x,y,t) = (\mathbf{u}(x,y,t),\mathbf{v}(x,y,t))$ , of





element-wise x and y-magnitudes, is then simply recovered from the spatial and temporal derivatives of the amplitude via solving the constancy equation<sup>28</sup>:

$$\frac{D\phi}{Dt} = \frac{\partial\phi}{\partial t} + \mathbf{v} \cdot \nabla\phi \quad \Rightarrow \quad \mathbf{v} = -\left(\left|\frac{\partial\phi}{\partial t}\right| / \|\nabla\phi\|^2\right) \nabla\phi \tag{Equation 1}$$

#### **Synchrony**

As is done with the classical Kuramoto order parameter,  $^{114}$  we compute the synchrony of instantaneous phases  $\theta$  as:

$$R_t = \frac{1}{N} \left| \sum_{xy} e^{i\theta(x,y,t)} \right|.$$
 (Equation 2)

Coherence is then the mean of this parameter across time, and metastability is the variance across time. <sup>115</sup> We compute this both globally, and locally across radii ranging from 1.750 cm to 7.875 cm in increments of 0.875. The minimum corresponds to one grid element and anything significantly larger than the maximum would entail areas that are predominantly outside of the scalp.

#### **Normalised velocity**

To characterise the collective motion of the field, we calculate the norm of the sum of the velocities divided by the sum of the norm of the velocities:

$$\Phi_t = \frac{\left\| \sum_{i=1}^N \overrightarrow{\mathbf{v}}_i \right\|}{\sum_{i=1}^N \left\| \overrightarrow{\mathbf{v}}_i \right\|},$$
 (Equation 3)

where N is the number of spatial elements in the field and  $\overrightarrow{\mathbf{v}}_i$  is the velocity the i-th element. If  $\Phi_t$  is close to 1, the vectors in the field are aligned and there is collective motion in a particular direction. <sup>42,116</sup>

#### **Heterogeneity**

To characterise the diversity of flows in the field we compute the heterogeneity, <sup>49</sup> as the mean over time of the standard deviation of wave propagation speeds. More formally:

$$H = \frac{1}{T} \sum_{t=1}^{T} \frac{1}{\mu(t)} \sqrt{\left(\frac{1}{N_t} \sum_{i=1}^{i=N_t} \left[ \left| \overrightarrow{\mathbf{v}}_i(t) \right| - \mu(t) \right]^2 \right)},$$
 (Equation 4)

where T is the total time,  $N_t$  the number of vectors at time t, and  $\mu(t) = \frac{1}{N_t} \sum_{i=1}^{N} \left| \overrightarrow{\mathbf{v}}_i(t) \right|$  the average speed at time t.

#### **Complex wave patterns**

Complex spatiotemporal waves are organised around critical points of stationarity. These singularities are of two main flavors, sources where flow arises, and sinks where flow gathers. First, we compute the divergence of the velocity field as the sum of the partial derivatives of each field component  $\frac{\partial u}{\partial x} + \frac{\partial v}{\partial y}$ . Singularities were then identified as extremal nested closed contours divergence. Tontours were run over 10 levels equally spaced between the 1st and 99th percentile of the divergence values. From this we compute the centroid of the singularity, the area of the contour occupied by the singularity, and the strength of the singularity as the magnitude of velocity divergence.

This allows us to calculate viscosity of flow, <sup>28</sup> which is taken as the product of the area and divergence of the singularities, more formally:

$$\nu = A \nabla \cdot \overrightarrow{\mathbf{v}}$$
. (Equation 5)

Thus, we recover the magnitude of resistance to flow, in units  $cm^2s^{-1}$  as in kinematic viscosity in fluid dynamics. Lower values indicate that waves can flow across space with greater ease, whereas higher values indicate that their distributed diffusion is restricted.

The nature of the singularities is then further characterised by the values of the trace  $(\tau)$  and the determinant  $(\Delta)$  of the Jacobian  $J^{37}$ , bilinearly interpolated from the neighboring grid elements on the scalp, which correspond to the divergence and curl of the field respectively:

$$J = \begin{pmatrix} \frac{\partial u}{\partial x} & \frac{\partial u}{\partial y} \\ \frac{\partial v}{\partial x} & \frac{\partial v}{\partial y} \end{pmatrix}$$
 (Equation 6)

# Cell Reports Article



Unstable singularities (sources) have  $\tau < 0$  and stable singularities (sinks) have  $\tau > 0$ . Nodes have  $\Delta > 0$  and  $\tau^2 > 4\Delta$ , focuses have  $\Delta > 0$  and  $\tau^2 < 4\Delta$ . Stable focuses are spiral-in waves, and unstable focuses are spiral-out waves. Lastly, saddles are characterised by  $\Delta < 0$ , and are usually formed by interactions between other waves.<sup>37</sup>

#### **Velocity field recurrence**

In order to characterise the recurrence of velocity fields we calculated their alignment matrix<sup>31</sup> via their mutual information (MI):

$$I(\mathbf{v}_i; \mathbf{v}_i) = H(\mathbf{v}_i) + H(\mathbf{v}_i) - H(\mathbf{v}_i, \mathbf{v}_i).$$
 (Equation 7)

Where H is the classic Shannon entropy function. We then shuffle the velocities spatially, compute the alignment matrix over 100 permutations and take the maximum MI value from each permutation and chose the 99th percentile of these values as a threshold for our empirical matrix. We treat this as the binary adjacency matrix A of a temporal graph, and characterise its structure.

#### **Recurrence network topology**

We first cluster nodes using Clauset-Newman-Moore greedy modularity maximization, <sup>119</sup> which finds the network partition that maximises the generalised modularity *Q*:

$$Q = \sum_{c=1}^{n} \left[ \frac{L_c}{m} - \gamma \left( \frac{k_c}{2m} \right)^2 \right].$$
 (Equation 8)

Where the sum iterates over all communities c,  $L_c$  is the number of intra-community edges, m is the total number of edges,  $k_c$  is the sum of the degrees in the community, and  $\gamma$  is the resolution parameter which we set to 1. 1.20

We also characterise the compactness of this recurrence network by computing the average of the inverse distances between nodes, i.e., its global efficiency:

$$E = \frac{1}{N(N-1)} \sum_{i \neq i \in V} \frac{1}{d_{ij}}$$
 (Equation 9)

where  $d_{ij}$  is the distance between the i-th and j-th nodes. In this case, higher global efficiency indicates that the network is compact and velocity fields are robust over time, whereas a lower global efficiency indicates that velocity fields exhibit less recurrence.

#### **Intrinsic timescales**

To identify the intrinsic timescale of the cortex we compute the average decay time of the auto-mutual information (*AMI*) function. That is, we find the mean lag at which the mutual information between neural signals and a delayed copy of themselves reaches a stable minima. To do so, we fit a straight line to the last third of the *AMI* function, and find the first time point that falls below the *AMI* value equal to the line's y-intercept. Longer intrinsic timescales indicate that a time series contains greater information about its own future, and shorter intrinsic timescales indicate that a timeseries is less history dependent. <sup>121</sup>

## **Separation rate**

To characterise the dynamical sensitivity of the system, we characterise the rate of divergence of similar points in phase space with the maximum Lyapunov exponent:

$$\lambda_{max} = \lim_{t \to \infty} \lim_{|\delta Z_0| \to 0} \frac{1}{t} \ln \frac{|\delta \mathbf{Z}(t)|}{|\delta \mathbf{Z}_0|},$$
 (Equation 10)

which we derive via Rosenstein's algorithm. Let  $\delta \mathbf{Z}(t)$  is the trajectory separation at time t. Briefly, the broadband amplitude envelope is produced by the Hilbert transform and its dynamics are reconstructed using Taken's embedding. The nearest neighbor of each time point is identified using the Euclidian distance, and their trajectories tracked. The separation rate is then the exponent of the curve of the mean logarithmic distance between these trajectories as a function of time, normalised by the sampling rate.

### **Energy landscape**

To characterise the shifts in the ability of the brain to orchestrate rapid global broadband reconfigurations, we follow previous work, 50,123,124 and characterise the energy landscape of neural dynamics through the statistical inference of the probability of an effect of a particular size. Effect is operationalised as mean-squared-displacement (MSD) in the Fisher z-scored amplitude envelope of broadband signals across the cortex:

$$MSD_{t,t_0} = \langle |x_{t_0+t} - x_{t_0}|^2 \rangle_r,$$
 (Equation 11)

where r is the number of electrodes. We compute the MSD with maximum lags of 1s, with 200 equally spaced initialisation points. As is done in statistical mechanics, we can then compute the energy E of the electrophysiological attractor basin via the natural





logarithm of the inverse probability, estimated via Gaussian kernel density estimation K. Following, <sup>124</sup> we compute this over MSD values between 0 and 5.

$$E = \ln \left( \frac{1}{\frac{1}{4n} \sum_{i=1}^{n} K\left(\frac{MSD_{t,t_0}}{4}\right)} \right)$$
 (Equation 12)

Thus, a highly probable relative change in neural activity corresponds to a putatively low energy requirement, and vice versa.

## **QUANTIFICATION AND STATISTICAL ANALYSIS**

Unless stated otherwise within the text, statistical tests were performed using paired two-tailed T-tests, with false discovery rate correction via Benjamini–Hochberg procedure, accompanied by Jeffrey-Zellner-Siow (JZS) Bayes Factor. \*, \*\*, \*\*\* indicates corrected p < .05,.01,.001. All group-level data are presented as mean  $\pm$  SEM.